© 2017. Published by The Company of Biologists Ltd | Journal of Cell Science (2017) 130, 1435-1449 doi:10.1242/jcs.198564

RESEARCH ARTICLE

Neuronal hyperactivity causes Na^+/H^+ exchanger-induced extracellular acidification at active synapses

Martina Chiacchiaretta[1,2,‡], Shahrzad Latifi[1,*,‡], Mattia Bramini[1], Manuela Fadda[2], Anna Fassio[1,2], Fabio Benfenati[1,2] and Fabrizia Cesca[1,§]

ABSTRACT

Extracellular pH impacts on neuronal activity, which is in turn an important determinant of extracellular H^+ concentration. The aim of this study was to describe the spatio-temporal dynamics of extracellular pH at synaptic sites during neuronal hyperexcitability. To address this issue we created ex.E^2GFP, a membrane-targeted extracellular ratiometric pH indicator that is exquisitely sensitive to acidic shifts. By monitoring ex.E^2GFP fluorescence in real time in primary cortical neurons, we were able to quantify pH fluctuations during network hyperexcitability induced by convulsant drugs or high-frequency electrical stimulation. Sustained hyperactivity caused a pH decrease that was reversible upon silencing of neuronal activity and located at active synapses. This acidic shift was not attributable to the outflow of synaptic vesicle H^+ into the cleft nor to the activity of membrane-exposed H^+ V-ATPase, but rather to the activity of the Na^+/H^+-exchanger. Our data demonstrate that extracellular synaptic pH shifts take place during epileptic-like activity of neural cultures, emphasizing the strict links existing between synaptic activity and synaptic pH. This evidence may contribute to the understanding of the physio-pathological mechanisms associated with hyperexcitability in the epileptic brain.

KEY WORDS: Acidic pH, Neural hyperexcitability, Active synapses, Experimental epilepsy, Na^+/H^+ exchanger, PH-sensitive GFP

INTRODUCTION

In biological systems, the H^+ concentration gradient between the intracellular and the extracellular environments plays a crucial role in several physiological processes (Chesler, 2003). In the central nervous system (CNS), the control of pH homeostasis is essential for the regulation of neurotransmission and neuronal excitability. While pH affects neural activity, neural activity causes pH alterations that vary in location and time (Chen and Chesler, 1992; Dulla et al., 2005; Makani and Chesler, 2007). Local pH changes occur in the brain during normal function (Chesler and Kaila, 1992; Magnotta et al., 2012), and neuronal firing causes both intracellular and extracellular pH shifts (Chesler, 2003; Chesler and Kaila, 1992; Kim and Trussell, 2009; Trapp et al., 1996). Rapid changes in intracellular pH have been observed at *Drosophila* nerve terminals during high-frequency *in vivo* activity (Caldwell et al., 2013; Rossano et al., 2013), while in the mammalian CNS, intense and synchronous activity of neural networks is accompanied by an initial alkalinization followed by a slower wave of acidification of the extracellular environment (DeVries, 2001; Du et al., 2014). A variety of ion channels, such as voltage-gated Ca^{2+} channels (Iijima et al., 1986), AMPA- and NMDA-type glutamate receptors (Lei et al., 2001; Tang et al., 1990; Traynelis and Cull-Candy, 1990) and $GABA_A$ receptors (Dietrich and Morad, 2010; Kaila, 1994) display sharp pH-sensitive conductance, indicating that pH itself can strongly influence neuronal excitability, neurotransmitter release and postsynaptic responses (Chen and Chesler, 1992; Dietrich and Morad, 2010; Makani and Chesler, 2007).

pH shifts are also associated with a number of pathological processes. Interstitial acidosis is present in several neuropathologies such as epilepsy (Gottfried and Chesler, 1996; Inamura et al., 1989; Krishtal et al., 1987; Somjen, 1984) and brain ischemia (Makani and Chesler, 2010; McCormick and Contreras, 2001; Nedergaard et al., 1991; Siesjo et al., 1996; Xiong and Stringer, 2000). The correlation between pH shifts and neuronal hyperexcitability is well established. However, because of the lack of accurate systems to measure the extracellular H^+ concentration, addressing the detailed events underlying pH-induced modulation of neural excitability is still a major challenge.

pH-sensitive microelectrodes generated some of the earliest measurements of both extracellular and intracellular pH, although their size and effects on tissue integrity strongly limit their widespread application. The use of fluorescent pH indicators opened new avenues to the study of pH fluctuations. The use of the extracellular ratiometric pH sensor SNARF allowed measurement of the local acidification in PC12 cells, which were stimulated by exposure to high K^+ concentrations (Shuba et al., 2008) and the stimulus-evoked non-quantal release of H^+ from vestibular hair cells at the cell–calyx afferent synapse (Highstein et al., 2014). More recently, genetically encoded fluorescent pH reporters that can be targeted to specific cellular compartments have been employed. One such indicator is a variant of the green fluorescent protein (GFP) obtained via specific mutagenesis, called 'ratiometric GFP', which is characterized by multiple excitation and emission maxima at distinct pH values (Bizzarri et al., 2006; Kuner and Augustine, 2000; Llopis et al., 1998). The absorption spectrum of GFP is widely used to measure the H^+ concentration in living organisms, and optimized versions of GFP for pH measurements have been generated (Kneen et al., 1998). Among various forms of GFP, ecliptic and super ecliptic pHluorins display no fluorescence when protonated, allowing sensitive detection of pH increases that are associated with biological processes (De Angelis et al., 1998; Miesenböck et al., 1998). GFP-based pH indicators have been extensively employed to study alterations of intracellular pH that are

[1]Center for Synaptic Neuroscience and Technology, Fondazione Istituto Italiano di Tecnologia, Largo Rosanna Benzi 10, Genova 16132, Italy. [2]Department of Experimental Medicine, University of Genova, Viale Benedetto XV 3, Genova 16132, Italy.
*Present address: Department of Neurology, David Geffen School of Medicine at UCLA, 710 Westwood Plaza, Los Angeles, CA 90095, USA.
‡These authors contributed equally to this work

§Author for correspondence (fabrizia.cesca@iit.it)

F.C., 0000-0003-2190-6314

Received 13 October 2016; Accepted 28 February 2017

Journal of Cell Science (2017) 130, 1435-1449 doi:10.1242/jcs.198564

related to network activity (Raimondo et al., 2012) and that can be used as markers of synaptic release (Miesenböck et al., 1998). However, only a few studies have employed them to monitor extracellular H^+ fluxes associated with neural excitability or under pathological conditions. Notably, very recently the super-ecliptic pHluorin has been targeted to synaptic compartments to detect release of H^+ that is associated with synaptic activity, suggesting a potential role of H^+ as an extracellular messenger (Du et al., 2014; Wang et al., 2014). However, superecliptic pHluorin, whose fluorescence is rapidly quenched in the acidic environment, is more sensitive to increases, rather than decreases, of pH.

The aim of the present study is to describe the spatio-temporal dynamics of extracellular pH fluctuations at synaptic sites during neuronal hyperexcitability. We employed E^2GFP to create a membrane-targeted extracellular ratiometric pH indicator. In contrast to other fluorescent pH sensors that are quenched at acidic pH, E^2GFP represents a very effective and exquisitely sensitive ratiometric pH indicator for acidic shifts. By monitoring variations of E^2GFP fluorescence in real time in primary hippocampal neurons, we were able to quantify pH fluctuations during network hyperactivity induced by convulsant drugs or high-frequency stimulation. Sustained neural hyperactivity caused a pH decrease that was specifically located at active synapses and was not attributable to the outflow of intravesicular H^+ into the cleft during intense exocytosis, but rather to the activation of the Na^+/H^+ exchanger. Our data could contribute to the understanding of the physio-pathological mechanisms associated with hyperexcitability in the epileptic brain.

RESULTS

Engineering and membrane targeting of a novel fluorescent sensor for extracellular pH

To engineer a genetically encoded indicator specifically sensitive to acidic pH shifts and targeted to the extracellular side of the plasma membrane, we inserted the E^2GFP sequence (Bizzarri et al., 2006) into the mammalian expression vector pDisplay™, which directs the encoded proteins to the cell surface. The resulting construct was named 'ex.E^2GFP' (Fig. 1A). The construct was subsequently cloned into a lentiviral vector under the control of the ubiquitous phosphoglycerate kinase (PGK) promoter to allow effective transduction of primary neurons. The subcellular localization of the probe was studied in the HEK293 cell line and primary cortical neurons. Membrane localization was observed in both cell types (Fig. 1B). To quantify the extent of membrane targeting of the probe in primary neurons, we labeled membranes with the lipophilic dye FM4-64fx and performed three-dimensional reconstruction using confocal microscopy. This analysis revealed that the vast majority of the probe was indeed localized to the plasma membrane, while the small pool of intracellular ex.E^2GFP is likely to correspond to the fraction of the protein that was being synthesized and translocated to the cell surface (Fig. 1C,D). To further demonstrate the plasma-membrane location of the probe, we performed subcellular fractionation of 17 days *in vitro* (DIV) neurons that had been infected with ex.E^2GFP, lysed and analyzed by western blotting using anti-GFP antibodies (Fig. 1E). ex.E^2GFP immunoreactivity was predominantly associated with the plasma-membrane-containing fraction P2, compared to the cytosolic/microsomal fraction S2.

Characterization of the ex.E^2GFP sensor

E^2GFP is ideally suited as a ratiometric biosensor as its emission can increase, decrease or be independent of pH based on the excitation wavelength, and its pK_a in the cytosolic form is about 6.8 (Bizzarri et al., 2006), thus very effective to detect pH changes just below the physiological range. We asked whether the optical properties of E^2GFP were affected by exposure to the extracellular environment. Primary cortical neurons were infected with ex.E^2GFP and fluorescence emission was evaluated at two extracellular pH values (5.8 and 7.4) using 405 and 488 nm as excitation wavelengths (λ_{ex}405 and λ_{ex}488, respectively) (Bizzarri et al., 2006, 2009) (Fig. 2A). This analysis revealed a much higher fluorescence intensity at acidic pH compared to physiological pH when ex.E^2GFP was excited at 405 nm, whereas an opposite behavior (albeit within a smaller dynamic range) was observed with 488 nm excitation (Fig. 2B). Thus, the extracellular targeting of E^2GFP does not alter its optical properties or its pH sensitivity.

Next, a calibration curve was produced by analyzing ex.E^2GFP fluorescence generated by switching the excitation wavelength between 405 and 488 nm and by systematically changing the extracellular pH from 5.7 to 7.8. To render the signal independent of the expression level of the protein, the ex.E^2GFP fluorescence ratio (λ_{ex}405/λ_{ex}488) was calculated and found to be strongly dependent on extracellular pH (Fig. 2C). Data were fitted according to a logistic sigmoidal function, with a pK_a value of 6.9±0.1 (mean±s.e.m.) that was very similar to that for soluble E^2GFP. This calibration curve was used to convert fluorescence ratios into absolute pH values throughout.

Neuronal hyperactivity causes localized extracellular acidic shifts in primary cultures

Several studies have addressed the question of how neuronal activity elicits changes in intracellular and extracellular H^+ concentration, sometimes yielding contrasting results (Caldwell et al., 2013; Chen and Chesler, 2015; Cichy et al., 2015; de Curtis et al., 1998; DeVries, 2001; Lu et al., 2012; Palmer et al., 2003; Xiong et al., 2000; Xiong and Stringer, 2000; Zhang et al., 2010; Zhao et al., 2011). We studied the effects of sustained heightened neural activity on the extracellular H^+ concentration by using *in vitro* models of epileptic-like network states characterized by synchronized neuronal discharges. Changes in fluorescence were monitored by live imaging (0.4 Hz frame rate) in primary cortical neurons that had been infected with lentiviruses encoding ex.E^2GFP, and pH values were subsequently extrapolated from ratio values using the calibration curve shown in Fig. 2C. A scheme of the time course of the experiments is shown in Fig. 3A – pH was first measured under baseline conditions (2 min), then network hyperactivity was induced by blocking $GABA_A$ receptors with bicuculline (30 µM), and cultures were imaged for 10 min. Thereafter, a selective blocker of voltage-gated Na^+ channels, tetrodotoxin (TTX; 300 nM), was added to suppress firing, and live imaging was continued for a further 10 min. During the time frame of the experiments, ex.E^2GFP fluorescence showed marked activity-dependent fluctuations, with no significant photobleaching (Fig. S1).

We found that *in vitro* seizure-like activity was associated with marked acidic pH transients in neurons. Interestingly, such fluorescence variations were observed both at the cell body level and along neurites of infected cells, where they mostly localized at synapse-like bouton structures (Fig. 3B; Movie 1). We thus monitored extracellular pH variations around these boutons and neuronal cell bodies. At both locations, acidic pH transients typically began at the onset of the hyperactivity triggered by the convulsant. After an initial delay, extracellular pH slowly but progressively decreased, reached a minimum acidic plateau 4-5 min after the beginning of the 'seizure-like' period and recovered towards baseline levels 4 min after termination of the seizure induced by TTX (Fig. 3C,D).

Journal of Cell Science (2017) 130, 1435-1449 doi:10.1242/jcs.198564

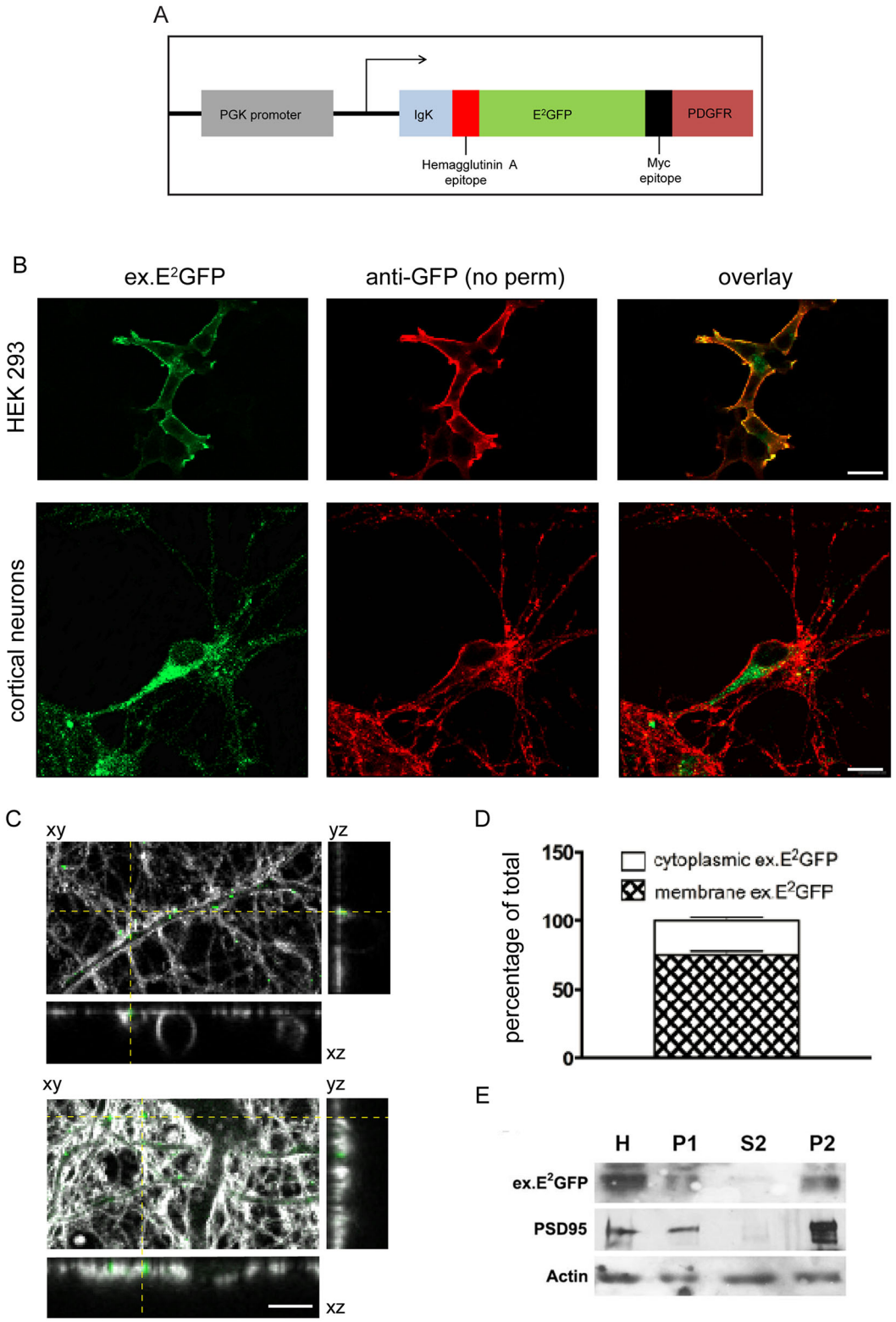

Fig. 1. Engineering and cellular localization of ex.E^{2}GFP. (A) Schematic illustration of the ex.E^{2}GFP lentiviral construct, showing the phosphoglycerate kinase (PGK) promoter, the murine IgK chain signal peptide, the hemagglutinin epitope, the E^{2}GFP sequence, the MYC epitope and the platelet-derived growth factor receptor (PDGFR) transmembrane domain. (B) Plasma membrane expression of ex.E^{2}GFP in HEK cells and primary cortical neurons. ex.E^{2}GFP expression in green; anti-GFP antibody in red, overlay in yellow shows colocalization. No perm, not permeabilized. Scale bars: 10 µm. (C,D) Representative images of primary cortical neurons expressing ex.E^{2}GFP (green) and stained with FM4-64fx (gray) for cell membrane visualization. *z*-stack images were acquired to quantify the percentage of ex.E^{2}GFP targeted to the plasma membrane (D). (E) Subcellular fractionation of 17 DIV neurons that had been infected with ex.E^{2}GFP, lysed and analyzed by western blotting using anti-GFP antibodies. PSD95 was used as marker of membrane distribution, and actin to verify equal loading. Immunoreactive bands corresponding to ex.E^{2}GFP are mostly present in the plasma-membrane-containing section P2. H, homogenate; P1, nuclear pellet; P2, crude synaptosomes; S2, supernatant of P2.

Journal of Cell Science (2017) 130, 1435-1449 doi:10.1242/jcs.198564

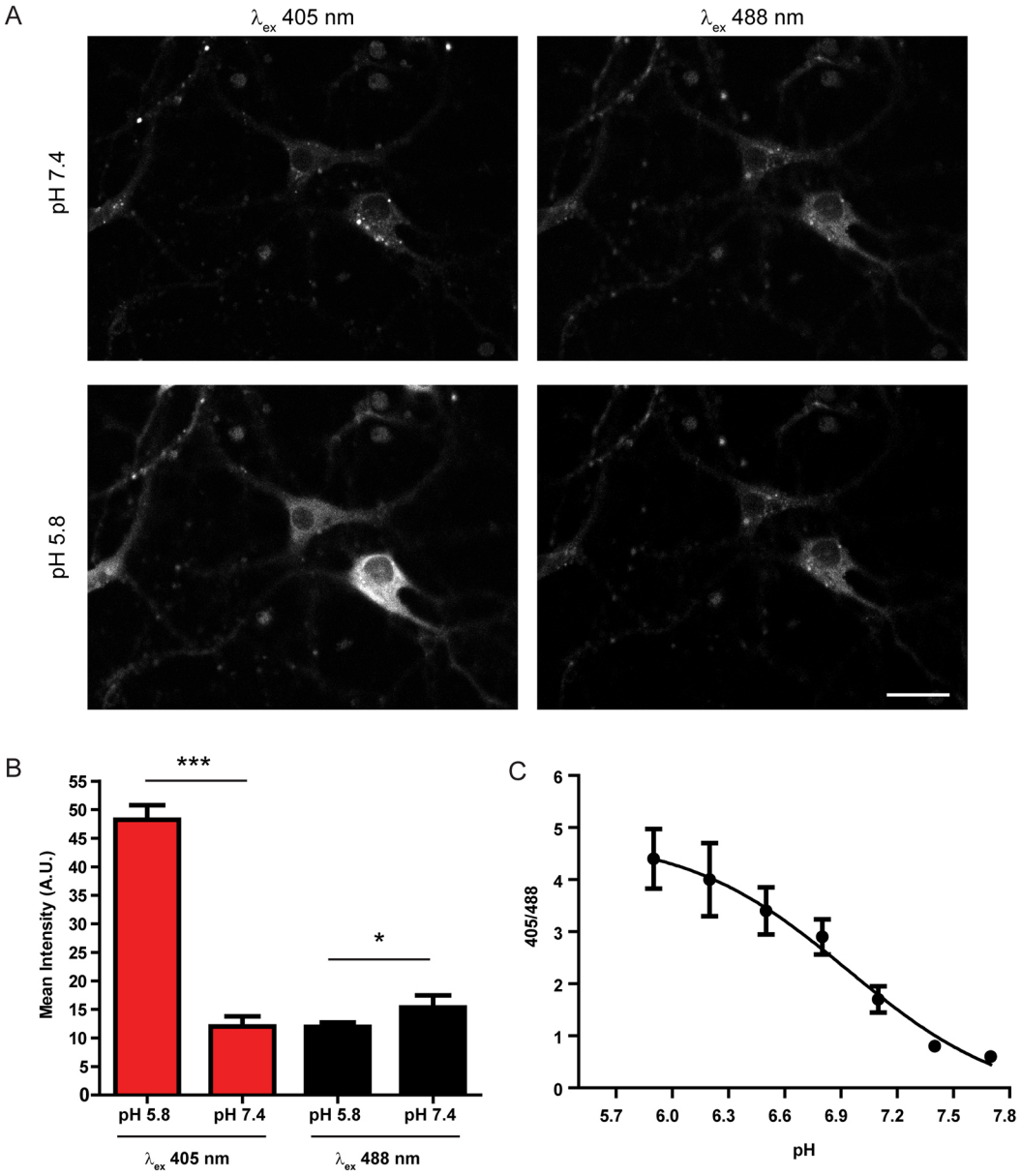

Fig. 2. Characterization of ex.E^{2}GFP. (A,B) Representative images and quantitative evaluation of ex.E^{2}GFP fluorescence intensity in cortical neurons at various extracellular pH values. The fluorophore was excited at 405 and 488 nm (λ_{ex}), and the emitted photons were collected within a single window (510-560 nm). Scale bar: 20 µm. The histograms show the mean±s.e.m. values of fluorescence intensity under the various λ_{ex} and pH conditions (*P<0.05, ***P<0.001, Student's *t*-test; n=15 cells from three independent experiments). (C) Calibration curve relating fluorescence intensity ratios to extracellular pH. Data (means±s.e.m. of n=15 cells from three independent experiments) were best-fit according to a sigmoidal dose–response equation: $y=-0.307+(4.83-0.372)/1+10^{6.9-x}$, R^2=0.99.

We subsequently asked how the time scale of increased neuronal firing compared to that of the acidic shift after addition of bicuculline. We cultured cortical neurons on 12-well multielectrode array (MEA) plates. Neurons were infected at DIV 10 and analyzed at DIV 15. The spiking rate was measured for 2 min under basal conditions, then bicuculline was added and the recording was continued for 10 min (Fig. 3E). In parallel, fluorescence was monitored in the same culture preparation. The bicuculline-induced increase in spiking rate was already observed 10 s after drug addition, while the pH decrease took about 4 min to reach a plateau. Thus, the increase in spiking activity happens first, followed by the pH decrease that appears to be a much slower process, which is likely to be due to the progressive extracellular accumulation of H^+ in the extracellular/synaptic space.

High-frequency electrical stimulation also triggers acidosis located at synaptic sites

To determine the variations of extracellular pH in response to a physiological electrical stimulation, cortical neurons expressing ex.E^{2}GFP were challenged with a stimulation of 1200 action potentials (APs) at 10 Hz (Fig. 4A; Movie 2). Electrical stimulation also triggered a fluorescence increase that was localized to discrete synapse-like boutons along the neurites. The acidic pH transient developed slowly during the stimulation and continued to reach an acidic plateau of pH 6.9±0.1 (mean±s.e.m.) about 50 s after the end of the stimulation (Fig. 4B,C). pH levels remained acidic until the end of the recording, showing only a slow and modest recovery. At the cell body level, the effects of electrical stimulation were much smaller and non statistically significant (Fig. 4B,C).

Journal of Cell Science (2017) 130, 1435-1449 doi:10.1242/jcs.198564

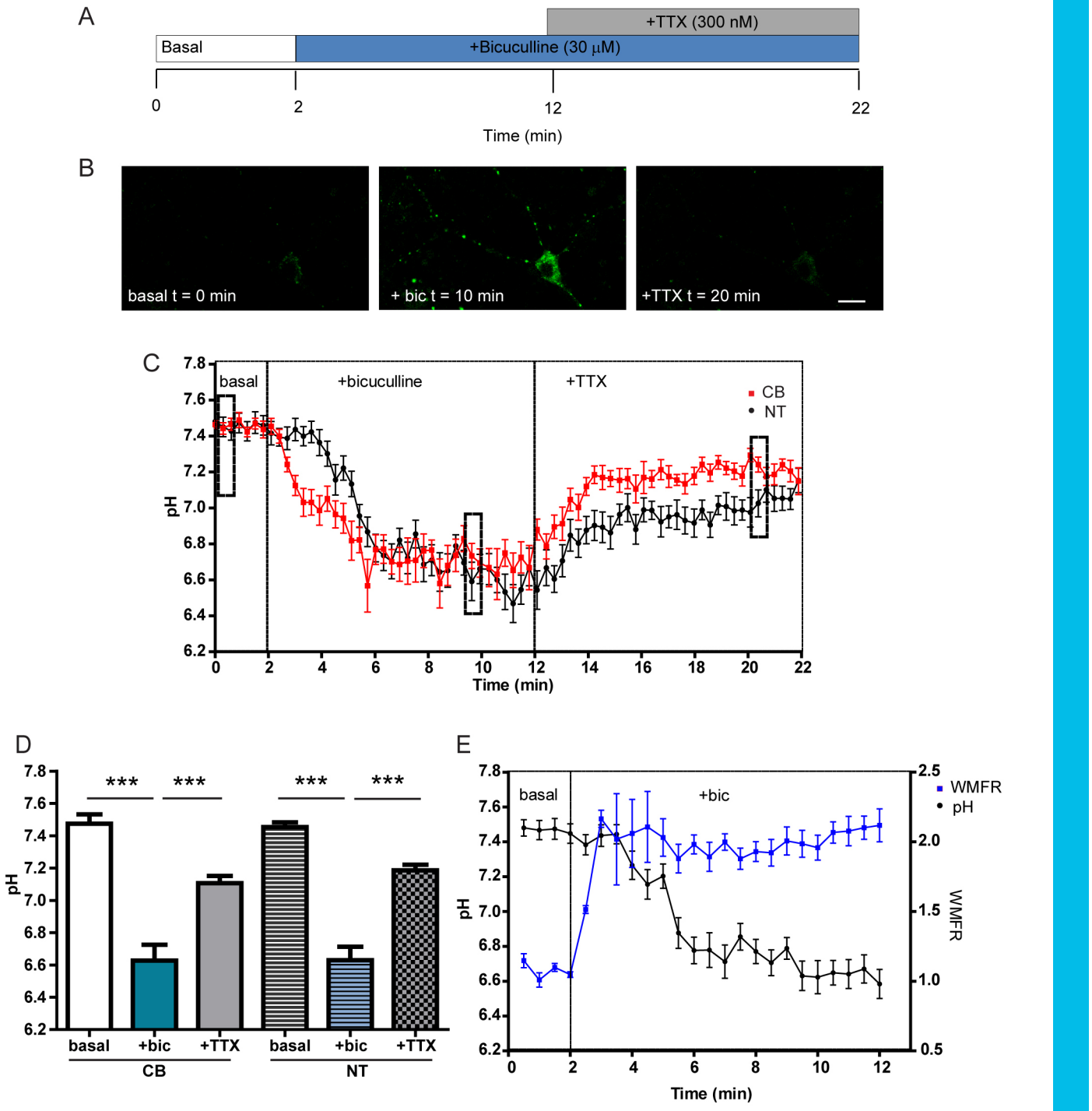

Fig. 3. Neural hyperactivity causes localized acidic shifts in primary neurons. (A) Schematic representation of the time course of a typical experiment with the addition of bicuculline (30 µM) and TTX (300 nM). (B) Representative images showing fluorescence intensities under basal conditions (t=0 min), after bicuculline treatment (t=10 min) and after TTX addition (t=20 min). Scale bar: 20 µm. (C) pH fluctuations as a function of time in cell bodies (CB, red squares; *n*=32) and nerve terminals (NT, black circles; *n*=20). Data are means±s.e.m. from at least three independent experiments. Values are shown for every sixth time point for clarity. Rectangles indicate values binned for the statistical analysis. (D) Quantification of pH shifts observed under basal conditions (basal), after treatment with bicuculline (+bic) and after TTX addition (+TTX) in nerve terminals and cell bodies. Mean±s.e.m. values were calculated by binning data from each independent trace as follows: basal, from 0 to 60 s; +bic, from 560 to 600 s; +TTX, from 1250 to 1318 s. ***P<0.001, one-way ANOVA followed by Bonferroni's multiple comparison test. (E) Network firing rate (weighted mean firing rate, WMFR, Hz; blue squares) and pH changes (black circles) were recorded under basal conditions (for 2 min) and after administration of bicuculline (for 10 min). Data are calculated from eight MEA dishes from three independent experiments.

To assess whether synaptic acidification is also present under basal conditions, we analyzed the live-imaging data corresponding to the 'basal' conditions of the various experiments. We identified single synapses and followed the behavior of ex.E^{2}GFP fluorescence over time in the corresponding regions of interest (ROIs). Interestingly, we found that 27% of the analyzed synapses did not show appreciable pH shifts (>0.1 pH units from basal), while 73% of

Journal of Cell Science (2017) 130, 1435-1449 doi:10.1242/jcs.198564

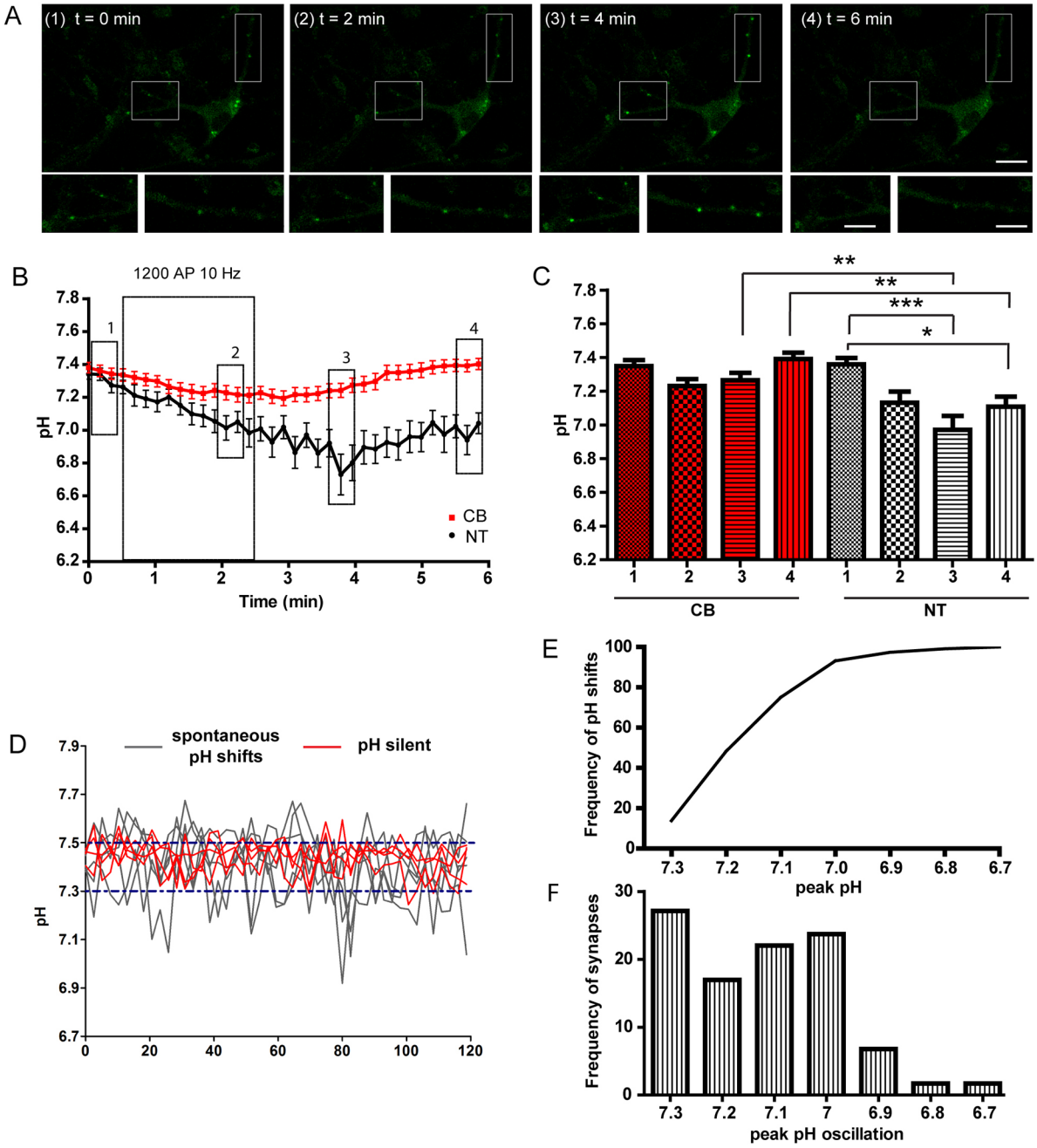

Fig. 4. High-frequency stimulation triggers slow-developing acidosis. (A) Electrical field stimulation (1200 APs, 10 Hz) was applied to cortical neurons that had been infected with ex.E^{2}GFP. Representative fluorescence images taken at λ_{ex}=405 nm from neurons under basal conditions (t=0 min), during the stimulus (t=2 min), after reaching the low pH plateau (t=4 min) and during the subsequent recovery (t=6 min). Scale bars: 20 µm and 10 µm for low and high (inset) magnifications, respectively. (B) pH fluctuation as a function of time in nerve terminals (NT, black squares; *n*=28) and cell bodies (CB, red circles; *n*=31) kept under basal conditions for 30 s, stimulated for 120 s with 1200 APs at 10 Hz and left to recover for 360 s. Data are means±s.e.m. from at least three independent experiments, with values shown every third time point for clarity. Rectangles indicate values binned for the statistical analysis. (C) Quantification of the extracellular pH shifts (means±s.e.m.) in response to high-frequency stimulation; values were calculated by binning data from each independent trace as follows: 1, 0-30 s; 2, 100-130 s; 3, 200-230 s; 4, 307-348 s. **P*<0.05, ***P*<0.01, ****P*<0.001, one-way ANOVA followed by Bonferroni's multiple comparison test. (D) Representative traces of synaptic pH changes under basal conditions in 14-17 DIV cortical neurons. Two populations of synapses were identified, characterized by spontaneous acidic shifts (pH<7.3; gray traces) or by substantially stable pH values (7.3<pH<7.5; red traces). (E) Cumulative distribution of the amplitude of pH shifts. (F) Frequency distribution of synapses as a function of peak pH oscillations observed during spontaneous activity. Data are from *n*=60 synapses from three independent experiments.

synapses displayed spontaneous pH oscillations that reached, in a small percentage of synapses, values between 6.6 and 6.9 (Fig. 4D-F). Thus, the majority of synapses under basal conditions display spontaneous activity levels of sufficient intensity to generate synaptic pH shifts.

Hyperactivity-induced pH shifts occur at synaptic sites

The punctate pattern of fluorescence observed in the neuropil upon induction of network hyperactivity was reminiscent of synaptic contacts. To investigate the subcellular distribution of ex.E^{2}GFP and unambiguously identify the sites of pH change,

Journal of Cell Science (2017) 130, 1435-1449 doi:10.1242/jcs.198564

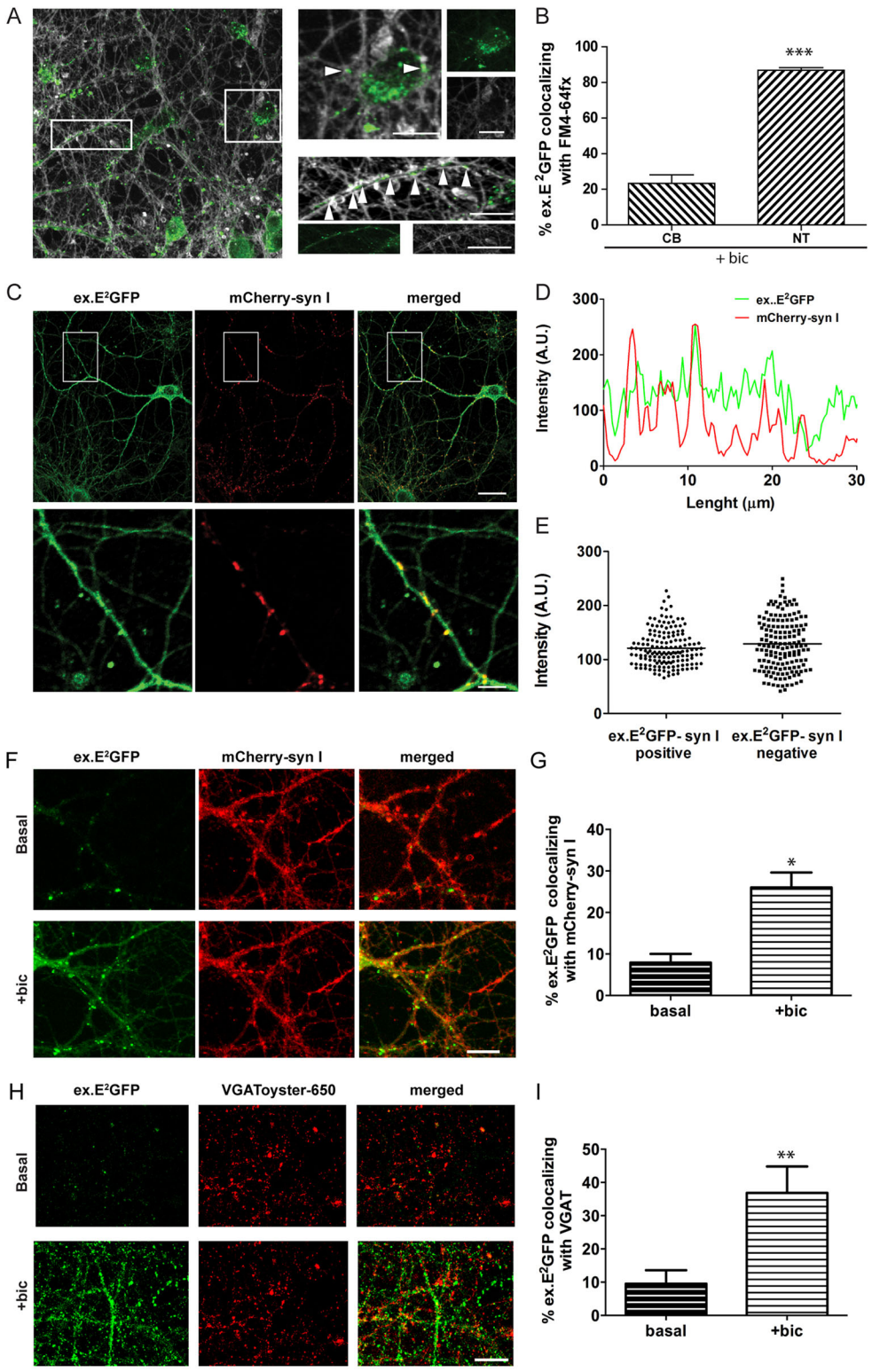

Fig. 5. See next page for legend.

we quantified the relative abundance of the probe in cell bodies and in synaptic boutons labeled by the lipophilic dye FM4-64fx upon bicuculline stimulation. Interestingly, the vast majority of ex.E^{2}GFP co-distributed with FM4-64fx-labeled puncta along neurites (Fig. 5A,B). However, it was unclear whether this was a specific activity-dependent synaptic acidification or the mere consequence of a non-specific accumulation of the sensor to synaptic boutons. To determine whether this was the case, primary cortical neurons were co-infected with lentiviruses expressing mCherry–synapsin-I (syn I), used as marker of presynaptic terminals (Cesca et al., 2010), and ex.E^{2}GFP. Comparable ex. E^{2}GFP intensity levels were observed under basal conditions at

Journal of Cell Science (2017) 130, 1435-1449 doi:10.1242/jcs.198564

Fig. 5. Acidic shifts are mainly localized to nerve terminals, and hyperactivity-induced acidification occurs at active synapses. (A) Representative images taken at λ_{ex}405 show overlay of ex.E^{2}GFP and FM4-64fx at low (left panel) and high (right panels) magnification. Scale bars: 20 µm (low magnification); 10 µm (high magnification). (B) Quantification of ex.E^{2}GFP-stained area colocalization with the cell membrane. Bar graph shows colocalization of ex.E^{2}GFP with FM4-64fx fluorescence for cell bodies (CB) and nerve terminals (NTs) under bicuculline stimulation. Means±s.e.m. of *n*=5 fields from three independent experiments. ***P<0.001, unpaired Student's *t*-test. (C) Primary cortical neurons co-infected with ex.E^{2}GFP- and mCherry–syn-I-expressing viruses were fixed and co-stained with anti-GFP and anti-mCherry antibodies to evaluate the synaptic versus extra-synaptic expression of ex.E^{2}GFP. Scale bars: 25 µm (low magnification, upper row); 5 µm (high magnification, lower row). (D) Representative intensity profiles of ex.E^{2}GFP and syn-I signals along neurites. (E) Quantification of the fluorescence intensity of ex.E^{2}GFP evaluated along neurites at synaptic (syn-I positive) and extra-synaptic (syn-I negative) regions. Data are calculated from *n*=160 ROIs from two independent experiments. Line represents mean. (F) Representative images of ex.E^{2}GFP (λ_{ex}405) and mCherry fluorescence under basal conditions (upper panels) and upon bicuculline (+bic) treatment (10 min, 30 µM; lower panels). The bicuculline-induced increase in ex.E^{2}GFP fluorescence (green channel) was mostly localized to syn-I-positive puncta (red channel). Scale bar: 10 µm. (G) Quantification of the synaptic localization of ex.E^{2}GFP fluorescence under basal conditions and after 10 min of bicuculline treatment. The fraction of the ex.E^{2}GFP-positive area that overlapped with mCherry–syn-I fluorescence under basal and bicuculline conditions evaluated as the Mander's coefficient is given as means±s.e.m. of *n*=5 fields from three independent experiments. *P<0.05, paired Student's *t*-test. (H) Representative images of ex.E^{2}GFP fluorescence and VGAT–Oyster650 live labeling in synaptic fields under basal conditions (upper panels) and upon bicuculline treatment (10 min, 30 µM; lower panels). Bicuculline-induced increase of ex.E^{2}GFP fluorescence (green channel) partially colocalized with VGAT-positive puncta (red channel). Scale bar: 10 µm. (I) Quantification of colocalization evaluated as the Mander's coefficient between ex.E^{2}GFP and VGAT–Oyster650 under basal conditions and after 10 min of bicuculline treatment (*n*=6 fields, from three independent experiments). **P<0.01, paired Student's *t*-test.

synaptic (i.e. synapsin positive) and extra-synaptic (i.e. synapsin negative) areas, thus confirming the ubiquitous targeting of the probe and the synaptic localization of the pH shifts (Fig. 5C-E). Because the expression of ex.E^{2}GFP is driven by the constitutive PGK promoter, the probe was expressed in both excitatory and inhibitory neurons. In fact, when primary cultures at various stages of maturation (between DIV 10 and 18) were double stained for GFP and markers of excitatory neurons (VGLUT1; also known as SLC17A7), inhibitory neurons (VGAT; also known as SLC32A1) and astrocytes (GFAP), ex.E^{2}GFP was found to be expressed in all three cell populations, although neuronal expression was predominant due to the paucity of glial cells under our culture conditions (Fig. S2).

Next, we investigated the specificity of the pH shifts for synaptic sites upon hyperactivity. A digital mask corresponding to presynaptic sites was built using the mCherry fluorescence, which was constant under resting and stimulated conditions (Fig. S3A), and the percent overlap of the ex.E^{2}GFP fluorescence with the masked area was calculated under basal conditions and upon bicuculline-induced hyperactivity. Stimulation caused an increase in ex.E^{2}GFP colocalization with mCherry–syn-I-positive puncta up to about 25-30% (Fig. 5F,G), demonstrating a massive recruitment of synaptic sites in the acidic response to the convulsant. By contrast, when the mask was built using the ex.E^{2}GFP fluorescence, which substantially increases in intensity and area upon stimulation (Fig. S3A), the ex.E^{2}GFP overlap on syn-I-labeled synaptic sites did not change (≈60%) (Fig. S3B), confirming the synaptic localization of ex.E^{2}GFP before and after stimulation, and the synaptic localization of the pH shifts.

Not all synapses labeled by synaptic markers such as syn I are functionally active (silent synapses). To relate ex.E^{2}GFP-positive puncta to active synapses, we co-infected hippocampal neurons with lentiviruses expressing ex.E^{2}GFP and synaptobrevin–pHluorin-mOrange2 (Syb2O), a marker of synaptic vesicle (SV) exo–endocytosis at active synaptic sites that has an emission spectrum that does not overlap with that of ex.E^{2}GFP (Ramirez et al., 2012). Upon electrical stimulation with 1200 APs at 10 Hz, ex.E^{2}GFP fluorescence and Syb2O fluorescence overlapped by approximately 60%, confirming the localization of the probe to active synapses (Fig. S3C,D).

We then asked whether the observed activity-dependent synaptic pH shifts were present in the whole synapse population, or whether they were preferentially localized to excitatory or inhibitory synapses. Primary cortical neurons were infected with ex.E^{2}GFP and live-labeled with VGAT–Oyster650, a specific marker of active inhibitory synapses (Fig. 5H). A digital mask corresponding to the active GABAergic boutons was built using the loaded VGAT–Oyster650 fluorescence, which remained constant under resting and stimulated conditions (Fig. S3E), and the percent overlap with the mask of the ex.E^{2}GFP fluorescence was calculated under basal conditions and upon bicuculline-induced hyperactivity. Stimulation caused an increase in ex.E^{2}GFP colocalization up to 35% with the active GABAergic synapses (Fig. 5I). By contrast, when the mask was built using the ex.E^{2}GFP fluorescence, which increases in intensity and area upon stimulation, the ex.E^{2}GFP overlap on VGAT-labeled synaptic sites was roughly constant (≈30%) (Fig. S3E-G).

Hyperactivity-induced pH shifts at synapses are not contributed by synaptic vesicle exocytosis

Neuronal activity triggers the mobilization of SVs, which are characterized by an acidic luminal pH due to the activity of the active H^+ transporter V-ATPase (Südhof, 2013). ex.E^{2}GFP, initially exposed on the plasma membrane at synapses, could get internalized into the acidic environment of endocytosed SVs. If this were the case, then the increase in ex.E^{2}GFP fluorescence would reflect the re-acidification of the endocytosed SVs, rather than a drop in the extracellular pH. To distinguish these two possibilities, we treated primary neurons with bafilomycin, a specific inhibitor of V-ATPase, which prevents re-acidification of SVs after exocytosis (Forgac, 1989). Pretreatment of neurons with bafilomycin before the addition of bicuculline did not affect either the bicuculline-induced acidification or the temporal profile of the pH decrease (Fig. 6A,B). These data demonstrate that acidification reflects a variation in the extracellular environment and that the release of H^+ from exocytosed SVs and/or the incorporation of the V-ATPase into the plasma membrane during SV exocytosis are not primarily involved.

Hyperactivity-induced pH shifts at synapses are due to the activity of the Na^+/H^+ exchanger

Since the pH shifts at synaptic sites are not attributable to release of H^+ from SVs into the synaptic cleft, we addressed the possibility that the secretion of H^+ during hyperactivity occurs via the activation of the Na^+/H^+ exchanger. We pretreated primary neurons with the Na^+/H^+ exchanger inhibitor amiloride before the addition of bicuculline (Fig. 7A,B). The treatment with amiloride alone induced a slight, but significant, extracellular alkalinization, confirming the constitutive activity of the Na^+/H^+ exchanger under basal conditions. Interestingly, when amiloride was combined with bicuculline stimulation, the extent of hyperactivity-induced extracellular acidification was significantly decreased, demonstrating the involvement of Na^+/H^+ exchangers in mediating the activity-

Journal of Cell Science (2017) 130, 1435-1449 doi:10.1242/jcs.198564

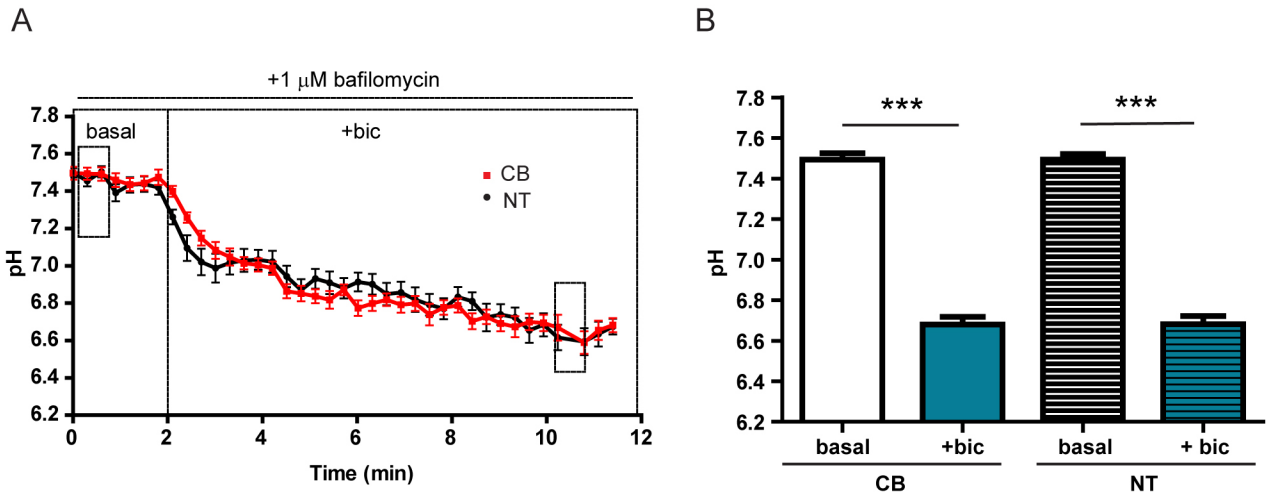

Fig. 6. The hyperactivity-induced pH shifts are not due to internalization of ex.E^{2}GFP. (A) Time-dependence of pH variations at synaptic puncta upon addition of bicuculline to neurons pretreated with 1 µM bafilomycin. The dynamics of pH changes are consistent with those obtained in the absence of bafilomycin (see Fig. 3). The graph displays traces of average ex.E^{2}GFP fluorescence plotted as pH values for cell bodies (CB, *n*=37) and nerve terminals (NT, *n*=39). Values (means±s.e.m. from at least three independent experiments) are shown for every sixth time point. Rectangles indicate values binned for the statistical analysis. (B) Quantification of pH shifts in the presence of bafilomycin. Values (means±s.e.m.) were calculated by binning data from each independent trace as follows: basal, from 0 to 46 s; +bic, from 637 to 683 s; ***P<0.001, one-way ANOVA followed by the Bonferroni's multiple comparison test.

induced synaptic pH shifts (Fig. 7C,D). As amiloride also inhibits Na^+/Ca^{2+} exchangers, we performed bicuculline treatment in the presence of 1 µM cariporide, a specific inhibitor of Na^+/H^+ exchanger isoform 1 (also known as SLC9A1), one of the most expressed Na^+/H^+ exchanger neuronal isoforms (Harguindey et al., 2013; Luo et al., 2005). We found that synaptic acidification was strongly inhibited under this experimental condition, indicating a major role of Na^+/H^+ exchanger 1 in the observed hyperactivity-induced synaptic acidification (Fig. 7E-H).

We also tested whether the blockade of bicuculline-induced extracellular acidification by amiloride was the result of an inhibition of network-firing activity by the drug. To this end, primary neurons were cultured on multi-well microelectrode arrays, and the network activity was analyzed in terms of firing rate, burst frequency and burst duration in the presence of the various treatments by following the same experimental protocol as that described in Fig. 7A (Fig. 8A). Notably, amiloride alone, bicuculline alone and amiloride+bicuculline all increased both the firing and the bursting frequencies (Fig. 8B-E), although acidification occurred only with bicuculline alone. The excitatory effect of amiloride on network activity confirms previous observations of a reduction of the sensitivity of $GABA_A$ receptors toward GABA by amiloride (Fisher, 2002). Altogether, our results demonstrate the key role of the Na^+/H^+ exchanger in coupling firing activity with a shift in extracellular pH.

DISCUSSION

Extracellular pH has important effects on neuronal activity, and in turn neuronal activity is an important determinant of the extracellular H^+ concentration. H^+ released by the SVs during sustained activity acts as a pseudo-transmitter, modifying several regulators of excitatory and inhibitory synaptic transmission (Cho and von Gersdorff, 2014; Du et al., 2014; Wang et al., 2014). Extracellular acidification occurs in the brain with elevated neural activity and neuronal injury (Wemmie et al., 2013). In turn, several studies have demonstrated the pH sensitivity of synaptic components like voltage-gated Ca^{2+} channels (VGCCs) (Iijima et al., 1986), ligand-gated AMPA and NMDA receptors (Traynelis and Cull-Candy, 1990), and GABA receptors (GABARs) (Kaila, 1994). In addition, acid-sensing ion channels (ASICs) are activated by extracellular low pH and are associated with neuronal dysfunction or brain injury (Friese et al., 2007; Yin et al., 2013). However, most of the studies have been performed on brain slices by applying high-speed pH microelectrodes (Fedirko et al., 2006) or dyes (Shuba et al., 2008), which lack accurate spatial resolution to localize pH changes to restricted neuronal domains.

In this paper, we analyzed the dynamics of extracellular pH changes accompanying epileptic-like activity in primary neuronal networks. We engineered a genetically encoded ratiometric GFP-based pH sensor that provides high spatial and temporal resolution to quantify variations in extracellular pH. Superecliptic GFP (pHluorin) has been employed previously as an extracellular pH sensor when targeted to the synaptic cleft (Du et al., 2014; Wang et al., 2014). However, pHluorin is an excellent reporter of alkalinization but quenches very rapidly upon acidic pH shifts. We therefore focused our attention on E^{2}GFP (Bizzarri et al., 2006), a ratiometric GFP derivative that successfully allows the live monitoring of the changes of intracellular pH towards acidosis (Bizzarri et al., 2006; Raimondo et al., 2012). We fused E^{2}GFP to the N-terminus of the PDGF receptor transmembrane domain that exposes it on the extracellular side of the plasma membrane (ex. E^{2}GFP). We demonstrated that the exposure to the extracellular environment does not affect E^{2}GFP optical properties and pH sensitivity, and that the targeted pH sensor shows high photostability with negligible photobleaching. Such a chimera has several advantages, namely: (i) it is ubiquitously targeted to the plasma membrane, thus being potentially able to map acidification in any region of the neuronal network; (ii) it is a ratiometric sensor with opposing pH sensitivities depending on the excitation wavelength, thus allowing reporting of pH changes independently of the expression level; and (iii) when excited at 405 nm, its fluorescence increases as the pH drops, making it more precise and sensitive in evaluating acidification than the previously used pHluorins.

We characterized hyperactivity-induced acidification by performing chemical stimulation with bicuculline and by applying high-frequency electrical stimulation. Using chemical stimulation,

Journal of Cell Science (2017) 130, 1435-1449 doi:10.1242/jcs.198564

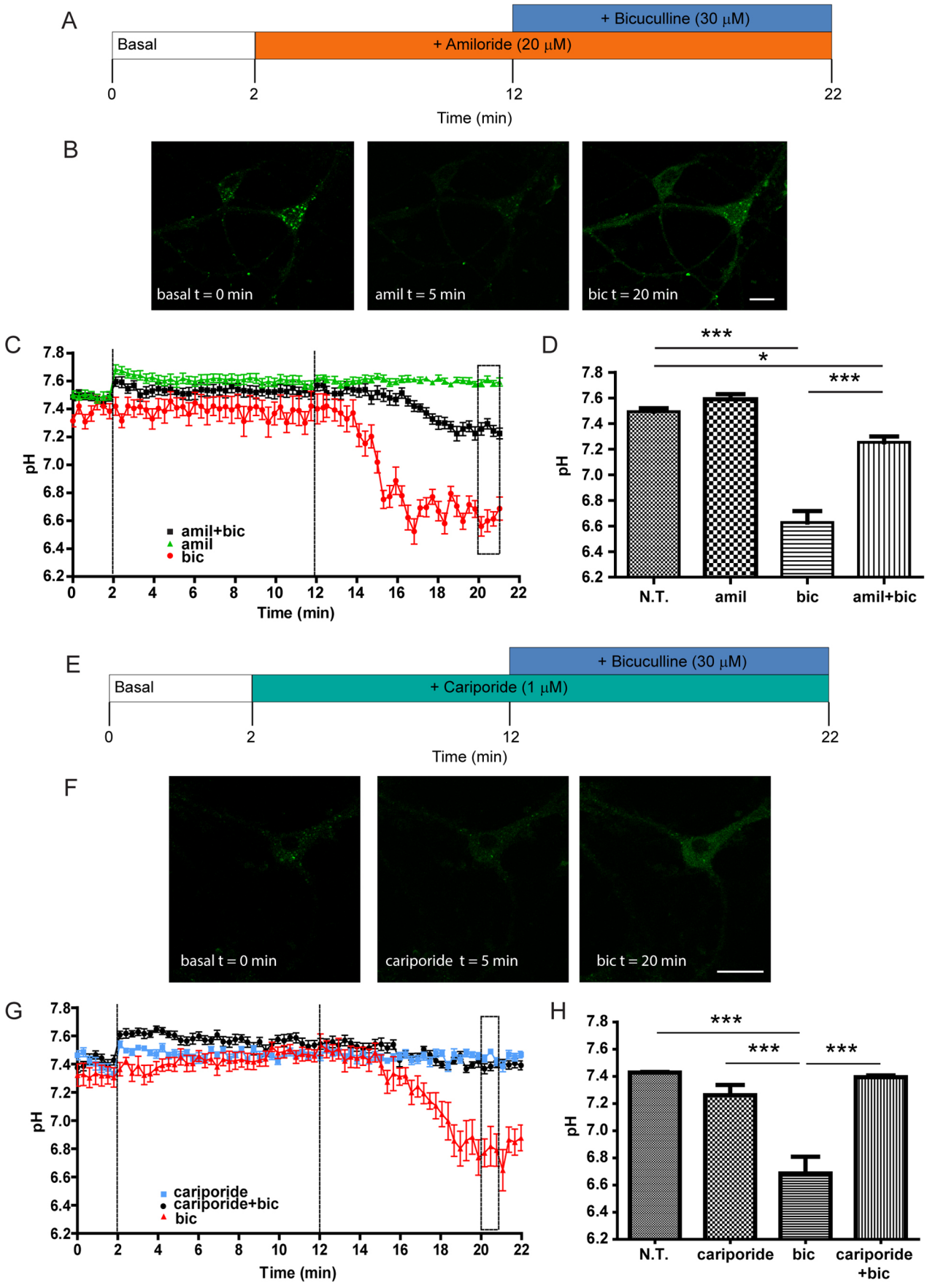

Fig. 7. See next page for legend.

Journal of Cell Science (2017) 130, 1435-1449 doi:10.1242/jcs.198564

Fig. 7. Na^+/H^+ exchanger channels modulate extracellular pH shifts. (A) Schematic representation of the time course of a typical experiment in which cells were treated with amiloride (20 µM) for 10 min before addition of bicuculline (30 µM). (B) Representative images showing the fluorescence intensity under basal conditions (t=0 min), after amiloride treatment (t=5 min) and 10 min after bicuculline addition (t=20 min). Scale bar: 20 µm. (C) Dynamics of pH fluctuations as a function of time in nerve terminals (n=20) from neurons treated with: (i) amiloride (amil, green triangles), (ii) bicuculline (bic, red circles) and (iii) amiloride+bicuculline (amil+bic, black squares). Non-treated (N.T.) samples were analyzed in parallel (trace not shown for clarity) and showed no appreciable pH changes over the course of the experiments. Data are means±s.e.m. from at least three independent experiments. Values are shown for every sixth time point. The rectangle indicates values binned for the statistical analysis. (D) Quantification of pH shifts observed after drug administration at plateau values from 1266 to 1318 s and compared to untreated samples (N.T.). Values (means±s.e.m.) were calculated by binning data from each independent trace; *P<0.05, ***P<0.001, one-way ANOVA followed by Bonferroni's multiple comparison test. (E) Schematic representation of the time course of a typical experiment in which cells were treated with cariporide (1 µM) for 10 min before addition of bicuculline (30 µM). (F) Representative images showing the fluorescence intensity under basal conditions (t=0 min), after cariporide treatment (t=5 min) and 10 min after bicuculline addition (t=20 min). Scale bar: 20 µm. (G) Dynamics of pH fluctuations in nerve terminals from neurons treated with: (i) cariporide (blue squares, n=19), bicuculline (bic, red triangles, n=15), and (iii) cariporide +bicuculline (black circles n=18). Non-treated (N.T.) samples were analyzed in parallel (trace not shown for clarity) and showed no appreciable pH changes over the course of the experiments. Data are means±s.e.m. from at least two independent experiments. Values are shown for every sixth time point. The rectangle indicates values binned for the statistical analysis. (H) Quantification of pH shifts observed after drug administration at plateau values from 1200 to 1260 s and compared to untreated samples (N.T.). Values (means±s.e.m.) were calculated by binning data from each independent trace; ***P<0.001, one-way ANOVA followed by Bonferroni's multiple comparison test.

we observed a relatively slow build-up of extracellular acidification that occurred at both cell bodies and synaptic sites, and that slowly returned to neutral pH upon silencing of electrical activity with TTX, with no apparent pre- or post-alkalinization phases. By contrast, the more physiological electrical stimulation showed a slower and milder synaptic acidification specifically localized to synaptic boutons. Interestingly, our probe was sensitive enough to detect also smaller acidic shifts associated with spontaneous activity. While ex.E^2GFP, which is exquisitely sensitive to the acidic shifts, may not be ideal to monitor alkaline shifts, the novelty of our results lays in the following points: (i) the increased network firing causes acidification at cell bodies and synapses, in both excitatory and inhibitory neurons; (ii) acidification does not result from the endocytotic capture of the membrane-exposed probe by SVs; (iii) acidification is mostly contributed by the Na^+/H^+ exchanger.

The acidic shifts in synaptic pH occurring during intense neuronal activity imply quantal or non-quantal release of H^+ from neurons. In principle, this can occur through (i) exocytosis of SVs; (ii) exposure of V-ATPase on the plasma membrane; (iii) increased production of CO_2 and metabolic acids, such as lactate, that are externalized by monocarboxylate transporters; (iv) activation of Na^+/H^+ exchanger (mostly the Na^+/H^+ exchanger 1) that transports Na^+ into the cells and extrudes H^+; and (v) activation of Na^+-dependent anion (Cl^-/HCO_3^-) exchangers (such as SLC4A8 and SLC4A10) that transport Na^+ and HCO^{3-} into the cell and extrude H^+ and Cl^- (Sinning and Hubner, 2013). Moreover, a glial source of H^+ cannot be excluded (Grichtchenko and Chesler, 1994), although this is unlikely to be the case in our cultures, which are virtually devoid of glial cells.

The demonstration that reduction of extracellular pH occurs in synaptic regions is consistent with recent studies (Cho and von Gersdorff, 2014; Du et al., 2014; Highstein et al., 2014; Wang et al., 2014). The synaptic distribution of acidic shifts emphasizes that an alteration of synaptic transmission is the first step for the initiation and maintenance of ictal activity (Lazarevic et al., 2013). Release of SV protons into the synaptic cleft upon intense exocytosis has been recently proposed as a mechanism of protonergic transmission (Du et al., 2014; Wang et al., 2014). However, this was not the case under our experimental conditions as the long delay between the onset of the hyperactivity state and the acidic shift makes it unlikely that the un-buffering of SV-released H^+ upon SV fusion (DeVries, 2001) significantly contributes to the acidic shift. Moreover, blockade of SV acidification does not affect the kinetics or the extent of acidification, ruling out H^+ release by SVs or sustained exposure of SV V-ATPase on the plasma membrane. This discrepancy is likely to be due to the different experimental models used in the various studies – i.e. *in vitro* cultures of mouse cortical neurons (present study), zebrafish retinal neurons (Wang et al., 2014) and mouse amygdala neurons in acute brain slices (Du et al., 2014). In addition, we have specifically studied the pH shifts caused by epileptic-like activity, which are likely to rely on different mechanisms with respect to physiological network activity.

Amongst the other potential mechanisms of extracellular acidification, we focused on the Na^+/H^+ exchangers as several members of this family are known to contribute to the onset and maintenance of epilepsy and other developmental brain disorders (recently reviewed in Zhao et al., 2016). Our data indicate that acidification during ictal activity is mostly due to the Na^+/H^+ exchanger as the addition of the Na^+/H^+ exchanger blocker amiloride strongly reduced the bicuculline-induced synaptic acidification. Na^+/H^+ exchanger 1 is one of the main Na^+/H^+ exchanger isoforms expressed in the CNS, and mutations in it are known to cause epilepsy in mice (Bell et al., 1999; Cox et al., 1997). Na^+/H^+ exchanger 1 is activated in response to intracellular acidification, and in neurons, the consequent extrusion of H^+ into the confined space of the synaptic cleft could generate the acidic pH shifts that we observed in our cultures. The other main neuronal Na^+/H^+ exchanger isoform is Na^+/H^+ exchanger 5 (Diering et al., 2011; Diering and Numata, 2014); however, treatment with the specific Na^+/H^+ exchanger 1 inhibitor cariporide (Harguindey et al., 2013; Luo et al., 2005) virtually abolished the bicuculline-induced pH shifts, thus suggesting that Na^+/H^+ exchanger 1 is the main isoform involved in the observed synaptic acidification.

In summary, we describe a novel sensor for extracellular pH changes and use it to study the wave of extracellular acidification during hyperactivity of the neuronal network, which is independent of H^+ released by SVs and is mostly generated by the activity of Na^+/H^+ exchangers. These results underline the strict links between synaptic activity and synaptic pH. The extracellular sensor engineered in this study could be employed to better understanding of ionic dynamics under physiological and pathological conditions with high spatio-temporal precision.

MATERIALS AND METHODS

Reagents

All biochemical reagents and drugs were purchased from Sigma-Aldrich unless otherwise specified. Tissue culture reagents and media were from Gibco – Thermo Fisher Scientific or Sigma-Aldrich. The following primary antibodies were used: anti-GFP (Thermo Fisher Scientific, #A-11122, dilution 1:500; Synaptic Systems, #132004, dilution 1:500 for triple staining with anti-Homer and anti-Bassoon antibodies), anti-GFAP (Sigma-Aldrich, #G3893, dilution 1:500), anti-VGLUT1 (Synaptic Systems, Goettingen, Germany, #1350304, dilution 1:500), anti-mCherry (Clontech, #632543, dilution 1:500), anti-Homer (Synaptic Systems, #16011, dilution

Journal of Cell Science (2017) 130, 1435-1449 doi:10.1242/jcs.198564

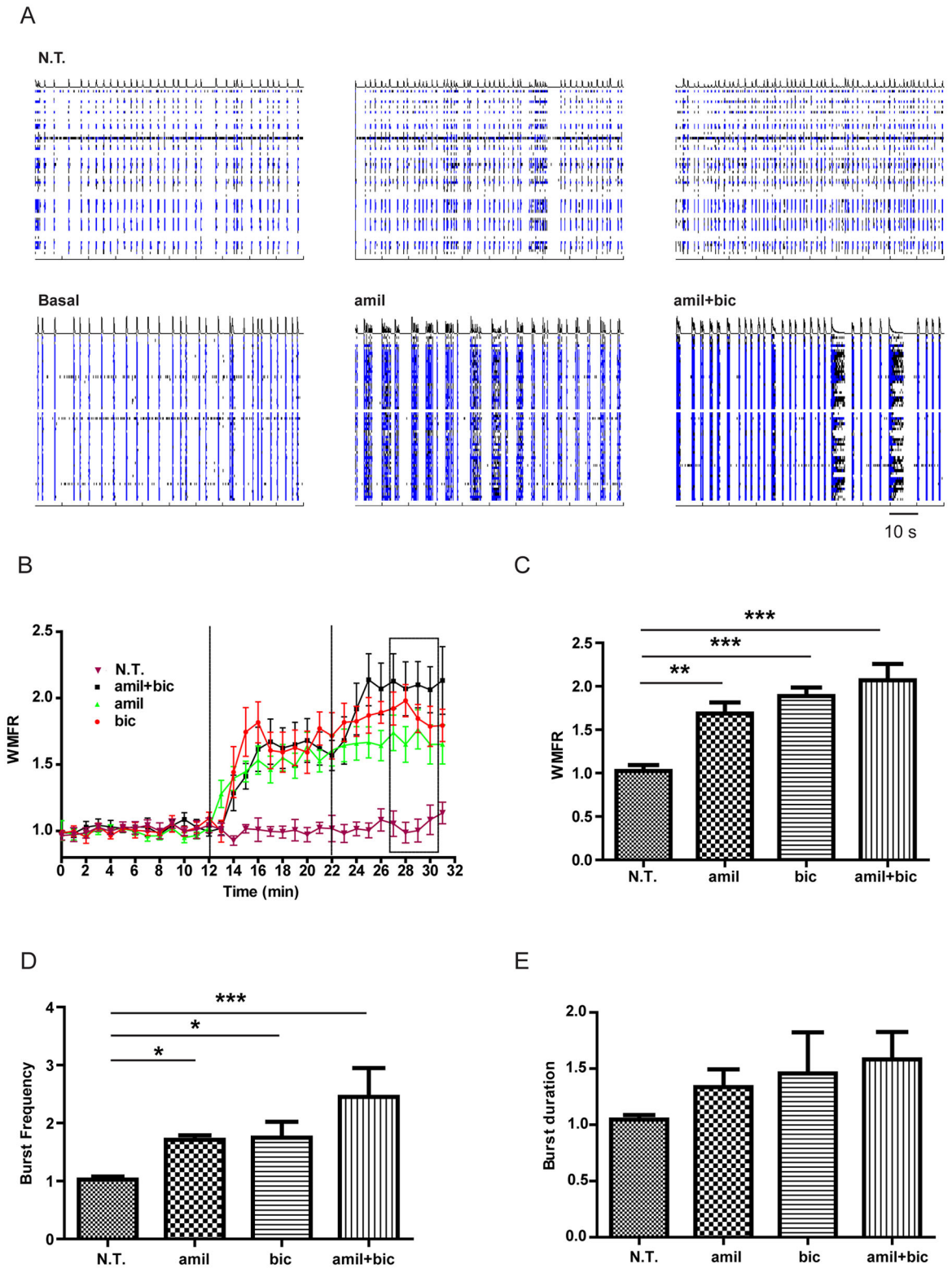

Fig. 8. Na^+/H^+ exchanger inhibition does not affect firing rate and burst frequency. (A) Representative raster plots of network activity recorded from 21 DIV cortical neurons treated with vehicle only (N.T.; upper panel) or with amiloride (amil) and amiloride+bicuculline (amil+bic, lower panel). Each row along the vertical axis represents an individual microelectrode of the MEA device for 100-s time windows (horizontal axis). (B) Dynamics of the weighted mean firing rate (WMFR) for neuronal cultures treated with: (i) vehicle (N.T., pink triangles), (ii) bicuculline for 20 min (bic, red circles), (iii) amiloride for 20 min (amil, green triangles) and (iv) amiloride for 10 min followed by bicuculline for 10 min (amil+bic, black squares). The rectangle indicates values binned for the analysis shown in C-E. (C) Bar graphs for WMFR were calculated by binning data from 1560 to 1860 s for each experimental group. Values (means±s.e.m.) were calculated from nine MEA dishes from three independent experiments. $^{**}P<0.01$, $^{***}P<0.001$, two-way ANOVA followed by Bonferroni's multiple comparison test. (D,E) Bar graphs representing the changes in bursting rate and burst duration, respectively, in the same experimental groups. Values (means±s.e.m.) were calculated from eight MEA dishes from three independent experiments. $^{*}P<0.05$, $^{***}P<0.001$, two-way ANOVA followed by Bonferroni's multiple comparison test.

Journal of Cell Science (2017) 130, 1435-1449 doi:10.1242/jcs.198564

1:500), anti-Bassoon (Synaptic Systems, #141002, dilution 1:500), anti-PSD95 (Synaptic Systems, #124011, dilution 1:1000) and anti-actin (Sigma-Aldrich, #A4700, dilution 1:1000) antibodies. Fluorophore-conjugated secondary antibodies were Alexa Fluor® 488-conjugated anti-rabbit (#A1108; dilution 1:1000), Alexa Fluor® 488-conjugated anti-guinea pig Alexa Fluor® 568-conjugated anti-mouse (#A-11004; dilution 1:1000), Alexa Fluor® 546-conjugated anti-rabbit (#A-11035; dilution 1:1000), Alexa Fluor® 647-conjugated anti-mouse (#A-21236; dilution 1:1000) and Alexa Fluor® 647-conjugated anti-guinea pig (#A-2145; dilution 1:1000) (all Thermo Fisher Scientific) antibodies.

Plasmids and transfection

The ex.E²GFP sequence was amplified from the pcDNA3.1+E²GFP plasmid (kindly provided by Dr Ranieri Bizzarri, Consiglio Nazionale delle Ricerche, Pisa, Italy) (Bizzarri et al., 2006) and inserted into the pDisplay™ vector (Thermo Fisher Scientific) between the BglII and PstI sites to obtain pDisplay-E²GFP (ex.E²GFP). The ex.E²GFP sequence was subsequently cloned into the pLenti-hPGK viral vector (kind gift of Drs Mario Amendola and Luigi Naldini, Tiget, Milan, Italy) between the AgeI and XhoI sites. The sequences of all constructs were verified by direct sequencing. Vectors were transiently transfected into cultured cells using Lipofectamine 2000 (Thermo Fisher Scientific).

Cell culture procedures

All experiments were performed in accordance with the guidelines established by the European Community Council (Directive 2010/63/EU of 22 September 2010) and approved by the Italian Ministry of Health. Human embryonic kidney cells (HEK293, purchased from American Type Culture Collection) and primary cortical cultures from wild-type C57Bl/6 mice (Charles River, Calco, Italy) were prepared and maintained following standard procedures (Baldelli et al., 2007; Cesca et al., 2015).

Viral transduction procedures

The production of VSV-pseudotyped third-generation lentiviruses was performed as previously described (De Palma and Naldini, 2002). Primary neurons were infected with ex.E²GFP alone or co-infected with mCherry–syn-I (Verstegen et al., 2014) at 10 DIV at 10 multiplicity of infection (MOI), and the experiments were performed 7-8 days post-infection (17-18 DIV). For multi-electrode array experiments, neurons were infected at 10 DIV, and recordings performed at 17-18 DIV. For pHluorin experiments, neurons were co-infected with synaptobrevin–pHluorin-m-Orange2 (Syb2O) (Ramirez et al., 2012) and ex.E^{2}GFP lentiviruses at 13 DIV, and optical recordings were performed at 17-18 DIV. Subcellular fractionation of transduced 17 DIV neurons was performed as previously described (Huttner et al., 1983).

Immunofluorescence and confocal microscopy

Immunohistochemistry on fixed cells was performed following standard procedures (Cesca et al., 2015). Coverslips were imaged by confocal microscopy (SP8, Leica Microsystems GmbH, Wetzlar, Germany) using a 63× (1.4 NA) magnification lens. Confocal images were analyzed with the Leica LAS AF software (Leica Application Suite Advance Fluorescence, version 3.3, Leica Microsystems). *z*-stack images for three-dimensional reconstruction were acquired in 300-nm steps, and offline analysis for colocalization quantification and determination of intensity profiles was performed using the JACoP plugin of the ImageJ software (Bolte and Cordelières, 2006).

Time-lapse live-cell imaging

For live-cell imaging experiments, an SP8 confocal laser-scanning microscope was used. The sequential excitation of ex.E^{2}GFP at 405 nm and 488 nm was achieved with a multiline argon laser. Emitted fluorescence was collected between 510 and 560 nm using a single photomultiplier tube (PMT) at a constant voltage. To verify fluctuations in laser intensity and bleaching of the probe, fluorescence was recorded in the absence of stimulation for the whole duration of a typical experiment. Neurons and cells were grown and maintained in 25-mm cover glasses and placed in a chamber with Tyrode solution (140 mM NaCl, 4 mM KCl, 1 mM $MgCl_2$, 2 mM $CaCl_2$, 10 mM glucose and 10 mM HEPES at pH 7.4). To build the calibration curve, neurons were incubated in solutions at controlled pH. For the acidic buffer (pH 5.8-6.2), HEPES was replaced with MES. Solutions were applied with a valve control perfusion system (Warner Instruments, Hamden, CT) after 2 min of baseline acquisition in physiological solution; 30 µM of bicuculline was added, followed by 300 µM of TTX. For amiloride experiments, after 2 min of baseline acquisition, 20 µM amiloride was added, followed by 30 µM bicuculline. For cariporide (Tocris, Avonmouth, Bristol, UK) experiments, after 2 min of baseline acquisition, 1µM cariporide was added, followed by 30 µM bicuculline. The acquisition rate was 0.4 Hz for each excitation wavelength. For field stimulation, time-lapse images were acquired every 2.58 s for 360 s. APs were evoked by passing 1-ms current pulses, yielding fields of 10 V/cm, through platinum-iridium electrodes using an AM 2100 stimulator (AM Systems, Carlsborg, WA). After 30 s of baseline acquisition, neurons were stimulated with a train of 1200 APs at 10 Hz.

Image analysis

Confocal images were analyzed with the Leica LAS X software. First, ROIs were chosen for each image. For cell bodies (CBs), the area of each ROI was 5 µm^2, while for nerve terminals (NTs) it was 2 µm^2, located on the center of mass of each nerve terminal. Fluorescence intensity ratios (R) were calculated according to the equation below:

$$R = \frac{MV(\lambda_x 405 - \lambda_e 510 - 560) - MV\,(background)}{MV(\lambda_x 488 - \lambda_e 510 - 560) - MV\,(background)}$$

where mean value, MV, is the average pixel intensity for each ROI and λ_x–λ_e is the excitation (collection) wavelength. pH values were calculated by fitting each average fluorescence intensity trace with the sigmoidal dose–response equation below:

$$y = -0.307 + \frac{(4.83 - 0.372)}{1 + 10^{6.9-x}}$$

Images were acquired with constant gain and exposure times across all experiments.

MEA recordings

Dissociated cortical neurons were plated onto 12-well planar MEAs (768-GL1-30Au200 from Axion BioSystems, Atlanta, GA), comprising 768 electrodes in 12 wells (64 electrodes/well). Extracellular spontaneous activity was recorded throughout the experiment and analyzed as previously described (Cesca et al., 2015; Chiappalone et al., 2009). Data were analyzed using the Neural metric tool (Axion Biosystems, Atlanta, GA).

Quantitative live-cell imaging for mCherry–syn-I, VGAT–Oyster650 and pHluorin experiments

Neurons co-expressing mCherry–syn-I and ex.E^{2}GFP were kept in a stimulation chamber (Warner Instruments, Hamden, CT) and imaged in Tyrode's solution. Bicuculline (30 µM) was added to the medium, and images were acquired after 10 min incubation using an SP8 fluorescence confocal laser-scanning microscope as described above. Five fields were analyzed using the JaCoP plug-in of ImageJ (Bolte and Cordelières, 2006).

For pHluorin experiments, neurons co-expressing Syb2O and ex.E^{2}GFP were kept in a stimulation chamber and imaged in physiological solution. The chamber was positioned on the stage of an IX-81 motorized inverted epifluorescence microscope (Olympus, Tokyo, Japan). An MT20 Hg-Xe lamp (Olympus, Tokyo, Japan) was used as a light source with 480±20 nm excitation, 495 nm dichroic and 525±50 nm emission filters to detect ex. E^{2}GFP signal. 560±40 nm excitation, 585 nm dichroic and 630±75 nm emission filters were instead used to detect the Syb2O signal. An electrical stimulation of 400 APs at 20 Hz was delivered to visualize active synapses. Images were acquired with an Hamamatsu Orca-ER CCD camera (Hamamatsu Photonics, Hamamatsu City, Japan) using an UplanSapo 60×1.35 NA oil immersion objective (Olympus, Tokio, Japan) and the software Excellence RT (Olympus, Tokyo, Japan). Fields expressing both signals were analyzed to evaluate the colocalization under basal and stimulated conditions; 11 fields were analyzed using the JaCoP plugin of ImageJ (Bolte and Cordelières, 2006).

Labeling with VGAT–Oyster650 (Synaptic Systems, Goettingen, Germany; #131103; dilution 1:200) was performed by incubating ex. E^2GFP-infected neurons for 20 min at 37°C under 5% CO_2 to load the dye into inhibitory presynaptic terminals through spontaneous activity. For basal conditions, images were acquired in Tyrode's solution. For the hyperexcited state, 30 µM bicuculline was added to the medium, and images were acquired after 10 min of incubation. Experiments were performed on an SP8 fluorescence confocal laser-scanning microscope, as described above. For all experiments, colocalization was analyzed by generating Manders' colocalization coefficients (Manders et al., 1992).

Statistical analysis

Data are expressed as means±s.e.m. for the number of cells (n) and mouse preparations detailed in the figure legends. Normal distribution of data was assessed using D'Agostino-Pearson's normality test (for $n>8$ values/experimental group) or the Kolmogorov–Smirnov test ($n<8$ values/experimental group). To compare two normally distributed sample groups, a paired or unpaired Student's t-test was used. To compare more than two normally distributed sample groups, one- or two-way ANOVA, followed by the Bonferroni's multiple comparison test, was used. α levels for all tests were 0.05% (95% confidence intervals). Statistical analysis was performed using Origin Pro 9.1 (OriginLab Corp., Northampton, MA) and GraphPad Prism 5 (GraphPad Software) software.

Acknowledgements

We thank Dr Kavalali (Department of Neuroscience, The University of Texas Southwestern Medical Center, Dallas, TX) for the synaptobrevin–Orange2 constructs, Dr Naldini (Tiget, Milan, Italy) for lentiviral constructs and protocols, and Drs Nanni and Mehili (Istituto Italiano di Tecnologia, Genova, Italy) for assistance in the preparation of primary cultures. We are also grateful to Ms Donato for helping in the initial phases of the project and to Drs Moretti and Pecoraro for helping with the MEA experiments.

Competing interests

The authors declare no competing or financial interests.

Author contributions

M.C. and S.L. performed the cell and molecular biology studies and the live-imaging experiments and analyzed the data. M.B. performed image analysis and quantification. M.F. performed the SybO2 experiments. F.C. and A.F. supervised the live-imaging and cell biology experiments, analyzed data and contributed to paper writing. F.B. and F.C. designed and supervised research, wrote the paper and provided financial support for the study. F.B. and F.C. equally contributed to this study.

Funding

This study was supported by research grants from the European Commission (FP7 Integrating Project 'Desire', grant number 602531 and ITN 'ECMED' number 642881 to F.B.). The support of Fondazione Telethon (grant GGP13033 to F.B.), Fondazione Cariplo (grant 2013 0879 to F.B.), Compagnia di San Paolo (grant 2015-0546 to F.B.), and the Ministero della Salute Ricerca Finalizzata 2013 (to F.B.) is also acknowledged.

Data availability

Supplementary information

Supplementary information available online at
http://jcs.biologists.org/lookup/doi/10.1242/jcs.198564.supplemental

References

Baldelli, P., Fassio, A., Valtorta, F. and Benfenati, F. (2007). Lack of synapsin I reduces the readily releasable pool of synaptic vesicles at central inhibitory synapses. *J. Neurosci.* **27**, 13520-13531.

Bell, S. M., Schreiner, C. M., Schultheis, P. J., Miller, M. L., Evans, R. L., Vorhees, C. V., Shull, G. E. and Scott, W. J. (1999). Targeted disruption of the murine Nhe1 locus induces ataxia, growth retardation, and seizures. *Am. J. Physiol.* **276**, C788-C795.

Bizzarri, R., Arcangeli, C., Arosio, D., Ricci, F., Faraci, P., Cardarelli, F. and Beltram, F. (2006). Development of a novel GFP-based ratiometric excitation and emission pH indicator for intracellular studies. *Biophys. J.* **90**, 3300-3314.

Bizzarri, R., Serresi, M., Luin, S. and Beltram, F. (2009). Green fluorescent protein based pH indicators for in vivo use: a review. *Anal. Bioanal. Chem.* **393**, 1107-1122.

Bolte, S. and Cordelières, F. P. (2006). A guided tour into subcellular colocalization analysis in light microscopy. *J. Microsc.* **224**, 213-232.

Caldwell, L., Harries, P., Sydlik, S. and Schwiening, C. J. (2013). Presynaptic pH and vesicle fusion in Drosophila larvae neurones. *Synapse* **67**, 729-740.

Cesca, F., Baldelli, P., Valtorta, F. and Benfenati, F. (2010). The synapsins: key actors of synapse function and plasticity. *Prog. Neurobiol.* **91**, 313-348.

Cesca, F., Satapathy, A., Ferrea, E., Nieus, T., Benfenati, F. and Scholz-Starke, J. (2015). Functional interaction between the scaffold protein Kidins220/ARMS and neuronal voltage-gated Na+ channels. *J. Biol. Chem.* **290**, 18045-18055.

Chen, J. C. and Chesler, M. (1992). pH transients evoked by excitatory synaptic transmission are increased by inhibition of extracellular carbonic anhydrase. *Proc. Natl. Acad. Sci. USA* **89**, 7786-7790.

Chen, H.-Y. and Chesler, M. (2015). Autocrine boost of NMDAR current in hippocampal CA1 pyramidal neurons by a PMCA-dependent, perisynaptic, extracellular pH shift. *J. Neurosci.* **35**, 873-877.

Chesler, M. (2003). Regulation and modulation of pH in the brain. *Physiol. Rev.* **83**, 1183-1221.

Chesler, M. and Kaila, K. (1992). Modulation of pH by neuronal activity. *Trends Neurosci.* **15**, 396-402.

Chiappalone, M., Casagrande, S., Tedesco, M., Valtorta, F., Baldelli, P., Martinoia, S. and Benfenati, F. (2009). Opposite changes in glutamatergic and GABAergic transmission underlie the diffuse hyperexcitability of synapsin I-deficient cortical networks. *Cereb. Cortex* **19**, 1422-1439.

Cho, S. and von Gersdorff, H. (2014). Proton-mediated block of Ca2+ channels during multivesicular release regulates short-term plasticity at an auditory hair cell synapse. *J. Neurosci.* **34**, 15877-15887.

Cichy, A., Ackels, T., Tsitoura, C., Kahan, A., Gronloh, N., Söchtig, M., Engelhardt, C. H., Ben-Shaul, Y., Müller, F., Spehr, J. et al. (2015). Extracellular pH regulates excitability of vomeronasal sensory neurons. *J. Neurosci.* **35**, 4025-4039.

Cox, G. A., Lutz, C. M., Yang, C.-L., Biemesderfer, D., Bronson, R. T., Fu, A., Aronson, P. S., Noebels, J. L. and Frankel, W. N. (1997). Sodium/hydrogen exchanger gene defect in slow-wave epilepsy mutant mice. *Cell* **91**, 139-148.

De Angelis, D. A., Miesenböck, G., Zemelman, B. V. and Rothman, J. E. (1998). PRIM: proximity imaging of green fluorescent protein-tagged polypeptides. *Proc. Natl. Acad. Sci. USA* **95**, 12312-12316.

de Curtis, M., Manfridi, A. and Biella, G. (1998). Activity-dependent pH shifts and periodic recurrence of spontaneous interictal spikes in a model of focal epileptogenesis. *J. Neurosci.* **18**, 7543-7551.

De Palma, M. and Naldini, L. (2002). Transduction of a gene expression cassette using advanced generation lentiviral vectors. *Methods Enzymol.* **346**, 514-529.

DeVries, S. H. (2001). Exocytosed protons feedback to suppress the Ca2+ current in mammalian cone photoreceptors. *Neuron* **32**, 1107-1117.

Diering, G. H. and Numata, M. (2014). Endosomal pH in neuronal signaling and synaptic transmission: role of Na(+)/H(+) exchanger NHE5. *Front Physiol.* **4**, 412.

Diering, G. H., Mills, F., Bamji, S. X. and Numata, M. (2011). Regulation of dendritic spine growth through activity-dependent recruitment of the brain-enriched Na(+)/H(+) exchanger NHE5. *Mol. Biol. Cell* **22**, 2246-2257.

Dietrich, C. J. and Morad, M. (2010). Synaptic acidification enhances GABAA signaling. *J. Neurosci.* **30**, 16044-16052.

Du, J. Y., Reznikov, L. R., Price, M. P., Zha, X.-M., Lu, Y., Moninger, T. O., Wemmie, J. A. and Welsh, M. J. (2014). Protons are a neurotransmitter that regulates synaptic plasticity in the lateral amygdala. *Proc. Natl. Acad. Sci. USA.* **111**, 8961-8966.

Dulla, C. G., Dobelis, P., Pearson, T., Frenguelli, B. G., Staley, K. J. and Masino, S. A. (2005). Adenosine and ATP link PCO2 to cortical excitability via pH. *Neuron* **48**, 1011-1023.

Fedirko, N., Svichar, N. and Chesler, M. (2006). Fabrication and use of high-speed, concentric h+- and Ca2+-selective microelectrodes suitable for in vitro extracellular recording. *J. Neurophysiol.* **96**, 919-924.

Fisher, J. L. (2002). Amiloride inhibition of gamma-aminobutyric acid(A) receptors depends upon the alpha subunit subtype. *Mol. Pharmacol.* **61**, 1322-1328.

Forgac, M. (1989). Structure and function of vacuolar class of ATP-driven proton pumps. *Physiol. Rev.* **69**, 765-796.

Friese, M. A., Craner, M. J., Etzensperger, R., Vergo, S., Wemmie, J. A., Welsh, M. J., Vincent, A. and Fugger, L. (2007). Acid-sensing ion channel-1 contributes to axonal degeneration in autoimmune inflammation of the central nervous system. *Nat. Med.* **13**, 1483-1489.

Gottfried, J. A. and Chesler, M. (1996). Temporal resolution of activity-dependent pH shifts in rat hippocampal slices. *J. Neurophysiol.* **76**, 2804-2807.

Grichtchenko, I. and Chesler, M. (1994). Depolarization-induced acid secretion in gliotic hippocampal slices. *Neuroscience* **62**, 1057-1070.

Harguindey, S., Arranz, J. L., Polo Orozco, J. D., Rauch, C., Fais, S., Cardone, R. A. and Reshkin, S. J. (2013). Cariporide and other new and powerful NHE1 inhibitors as potentially selective anticancer drugs–an integral molecular/biochemical/metabolic/clinical approach after one hundred years of cancer research. *J. Transl. Med.* **11**, 282.

Highstein, S. M., Holstein, G. R., Mann, M. A. and Rabbitt, R. D. (2014). Evidence that protons act as neurotransmitters at vestibular hair cell-calyx afferent synapses. *Proc. Natl. Acad. Sci. USA* **111**, 5421-5426.

Huttner, W. B., Schiebler, W., Greengard, P. and De Camilli, P. (1983). Synapsin I (protein I), a nerve terminal-specific phosphoprotein. III. Its association with synaptic vesicles studied in a highly purified synaptic vesicle preparation. *J. Cell Biol.* **96**, 1374-1388.

Iijima, T., Ciani, S. and Hagiwara, S. (1986). Effects of the external pH on Ca channels: experimental studies and theoretical considerations using a two-site, two-ion model. *Proc. Natl. Acad. Sci. USA* **83**, 654-658.
Inamura, K., Smith, M.-L., Hansen, A. J. and Siesjö, B. K. (1989). Seizure-induced damage to substantia nigra and globus pallidus is accompanied by pronounced intra- and extracellular acidosis. *J. Cereb. Blood Flow Metab.* **9**, 821-829.
Kaila, K. (1994). Ionic basis of GABAA receptor channel function in the nervous system. *Prog. Neurobiol.* **42**, 489-537.
Kim, Y. and Trussell, L. O. (2009). Negative shift in the glycine reversal potential mediated by a Ca2+- and pH-dependent mechanism in interneurons. *J. Neurosci.* **29**, 11495-11510.
Kneen, M., Farinas, J., Li, Y. and Verkman, A. S. (1998). Green fluorescent protein as a noninvasive intracellular pH indicator. *Biophys. J.* **74**, 1591-1599.
Krishtal, O. A., Osipchuk, Y. V., Shelest, T. N. and Smirnoff, S. V. (1987). Rapid extracellular pH transients related to synaptic transmission in rat hippocampal slices. *Brain Res.* **436**, 352-356.
Kuner, T. and Augustine, G. J. (2000). A genetically encoded ratiometric indicator for chloride: capturing chloride transients in cultured hippocampal neurons. *Neuron* **27**, 447-459.
Lazarevic, V., Pothula, S., Andres-Alonso, M. and Fejtova, A. (2013). Molecular mechanisms driving homeostatic plasticity of neurotransmitter release. *Front Cell Neurosci* **7**, 244.
Lei, S., Orser, B. A., Thatcher, G. R., Reynolds, J. N. and MacDonald, J. F. (2001). Positive allosteric modulators of AMPA receptors reduce proton-induced receptor desensitization in rat hippocampal neurons. *J. Neurophysiol.* **85**, 2030-2038.
Llopis, J., McCaffery, J. M., Miyawaki, A., Farquhar, M. G. and Tsien, R. Y. (1998). Measurement of cytosolic, mitochondrial, and Golgi pH in single living cells with green fluorescent proteins. *Proc. Natl. Acad. Sci. USA* **95**, 6803-6808.
Lu, Y., Yi, L., Liu, D., Li, J., Sun, L. and Zhang, Z. (2012). Alkalosis leads to the over-activity of cortical principal neurons. *Neurosci. Lett.* **525**, 117-122.
Luo, J., Chen, H., Kintner, D. B., Shull, G. E. and Sun, D. (2005). Decreased neuronal death in Na+/H+ exchanger isoform 1-null mice after in vitro and in vivo ischemia. *J. Neurosci.* **25**, 11256-11268.
Magnotta, V. A., Heo, H. Y., Dlouhy, B. J., Dahdaleh, N. S., Follmer, R. L., Thedens, D. R., Welsh, M. J. and Wemmie, J. A. (2012). Detecting activity-evoked pH changes in human brain. *Proc. Natl. Acad. Sci. USA* **109**, 8270-8273.
Makani, S. and Chesler, M. (2007). Endogenous alkaline transients boost postsynaptic NMDA receptor responses in hippocampal CA1 pyramidal neurons. *J. Neurosci.* **27**, 7438-7446.
Makani, S. and Chesler, M. (2010). Rapid rise of extracellular pH evoked by neural activity is generated by the plasma membrane calcium ATPase. *J. Neurophysiol.* **103**, 667-676.
Manders, E. M., Stap, J., Brakenhoff, G. J., van Driel, R. and Aten, J. A. (1992). Dynamics of three-dimensional replication patterns during the S-phase, analysed by double labelling of DNA and confocal microscopy. *J. Cell Sci.* **103**, 857-862.
McCormick, D. A. and Contreras, D. (2001). On the cellular and network bases of epileptic seizures. *Annu. Rev. Physiol.* **63**, 815-846.
Miesenböck, G., De Angelis, D. A. and Rothman, J. E. (1998). Visualizing secretion and synaptic transmission with pH-sensitive green fluorescent proteins. *Nature* **394**, 192-195.
Nedergaard, M., Goldman, S. A., Desai, S. and Pulsinelli, W. A. (1991). Acid-induced death in neurons and glia. *J. Neurosci.* **11**, 2489-2497.
Palmer, M. J., Hull, C., Vigh, J. and von Gersdorff, H. (2003). Synaptic cleft acidification and modulation of short-term depression by exocytosed protons in retinal bipolar cells. *J. Neurosci.* **23**, 11332-11341.
Raimondo, J. V., Irkle, A., Wefelmeyer, W., Newey, S. E. and Akerman, C. J. (2012). Genetically encoded proton sensors reveal activity-dependent pH changes in neurons. *Front Mol. Neurosci.* **5**, 68.
Ramirez, D. M. O., Khvotchev, M., Trauterman, B. and Kavalali, E. T. (2012). Vti1a identifies a vesicle pool that preferentially recycles at rest and maintains spontaneous neurotransmission. *Neuron* **73**, 121-134.
Rossano, A. J., Chouhan, A. K. and Macleod, G. T. (2013). Genetically encoded pH-indicators reveal activity-dependent cytosolic acidification of Drosophila motor nerve termini in vivo. *J. Physiol.* **591**, 1691-1706.
Shuba, Y. M., Dietrich, C. J., Oermann, E., Cleemann, L. and Morad, M. (2008). Local extracellular acidification caused by Ca2+-dependent exocytosis in PC12 cells. *Cell Calcium* **44**, 220-229.
Siesjo, B. K., Katsura, K. and Kristian, T. (1996). Acidosis-related damage. *Adv. Neurol.* **71**, 209-233; discussion 234-6.
Sinning, A. and Hubner, C. A. (2013). Minireview: pH and synaptic transmission. *FEBS Lett.* **587**, 1923-1928.
Somjen, G. G. (1984). Acidification of interstitial fluid in hippocampal formation caused by seizures and by spreading depression. *Brain Res.* **311**, 186-188.
Südhof, T. C. (2013). Neurotransmitter release: the last millisecond in the life of a synaptic vesicle. *Neuron* **80**, 675-690.
Tang, C. M., Dichter, M. and Morad, M. (1990). Modulation of the N-methyl-D-aspartate channel by extracellular H+. *Proc. Natl. Acad. Sci. USA* **87**, 6445-6449.
Trapp, S., Lückermann, M., Kaila, K. and Ballanyi, K. (1996). Acidosis of hippocampal neurones mediated by a plasmalemmal Ca2+/H+ pump. *Neuroreport* **7**, 2000-2004.
Traynelis, S. F. and Cull-Candy, S. G. (1990). Proton inhibition of N-methyl-D-aspartate receptors in cerebellar neurons. *Nature* **345**, 347-350.
Verstegen, A. M. J., Tagliatti, E., Lignani, G., Marte, A., Stolero, T., Atias, M., Corradi, A., Valtorta, F., Gitler, D., Onofri, F. et al. (2014). Phosphorylation of synapsin I by cyclin-dependent kinase-5 sets the ratio between the resting and recycling pools of synaptic vesicles at hippocampal synapses. *J. Neurosci.* **34**, 7266-7280.
Wang, T.-M., Holzhausen, L. C. and Kramer, R. H. (2014). Imaging an optogenetic pH sensor reveals that protons mediate lateral inhibition in the retina. *Nat. Neurosci.* **17**, 262-268.
Wemmie, J. A., Taugher, R. J. and Kreple, C. J. (2013). Acid-sensing ion channels in pain and disease. *Nat. Rev. Neurosci.* **14**, 461-471.
Xiong, Z. Q. and Stringer, J. L. (2000). Extracellular pH responses in CA1 and the dentate gyrus during electrical stimulation, seizure discharges, and spreading depression. *J. Neurophysiol.* **83**, 3519-3524.
Xiong, Z. Q., Saggau, P. and Stringer, J. L. (2000). Activity-dependent intracellular acidification correlates with the duration of seizure activity. *J. Neurosci.* **20**, 1290-1296.
Yin, T., Lindley, T. E., Albert, G. W., Ahmed, R., Schmeiser, P. B., Grady, M. S., Howard, M. A. and Welsh, M. J. (2013). Loss of Acid sensing ion channel-1a and bicarbonate administration attenuate the severity of traumatic brain injury. *PLoS ONE* **8**, e72379.
Zhang, Z., Nguyen, K. T., Barrett, E. F. and David, G. (2010). Vesicular ATPase inserted into the plasma membrane of motor terminals by exocytosis alkalinizes cytosolic pH and facilitates endocytosis. *Neuron* **68**, 1097-1108.
Zhao, H., Cai, Y., Yang, Z., He, D. and Shen, B. (2011). Acidosis leads to neurological disorders through overexciting cortical pyramidal neurons. *Biochem. Biophys. Res. Commun.* **415**, 224-228.
Zhao, H., Carney, K. E., Falgoust, L., Pan, J. W., Sun, D. and Zhang, Z. (2016). Emerging roles of Na(+)/H(+) exchangers in epilepsy and developmental brain disorders. *Prog. Neurobiol.* **138-140**, 19-35.

SUPPLEMENTARY MATERIALS

Fig. S1 Chiacchiaretta et al

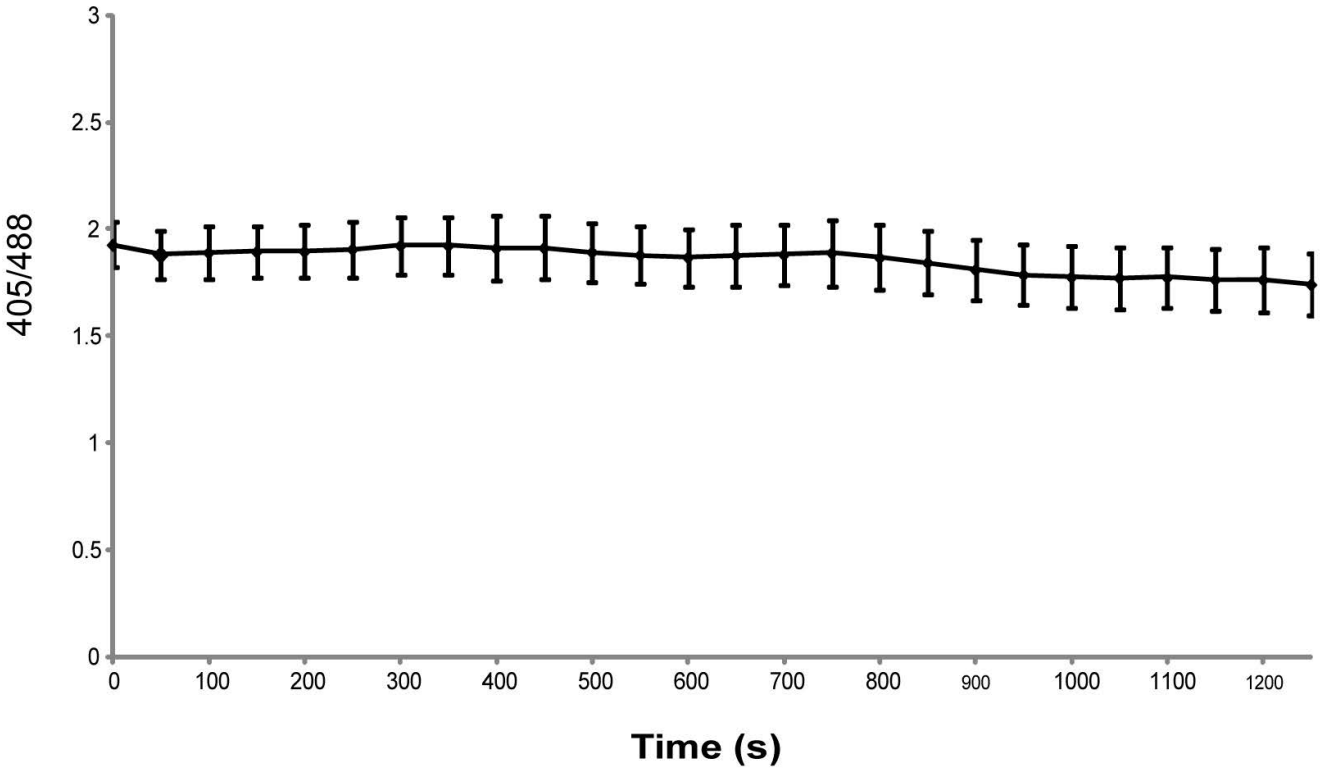

Figure S1. ex.E^{2}GFP fluorescence is not sensitive to photobleaching.

To quantify the extent of ex.E^{2}GFP photobleaching, changes in fluorescence intensity were followed for a period of time corresponding to our time-lapse experiments under constant pH (pH 6). Emitted photons were monitored by live imaging throughout the experiments at a frame rate of 0.1 Hz. For collecting excitation and emission, the same optical parameters were used as described for the calibration curve, and fluorescence ratios were calculated using the equation described in Materials and Methods. Values are means ± sem. No significant photobleaching was observed during the time course of the experiment.

Fig. S2 Chiacchiaretta et al

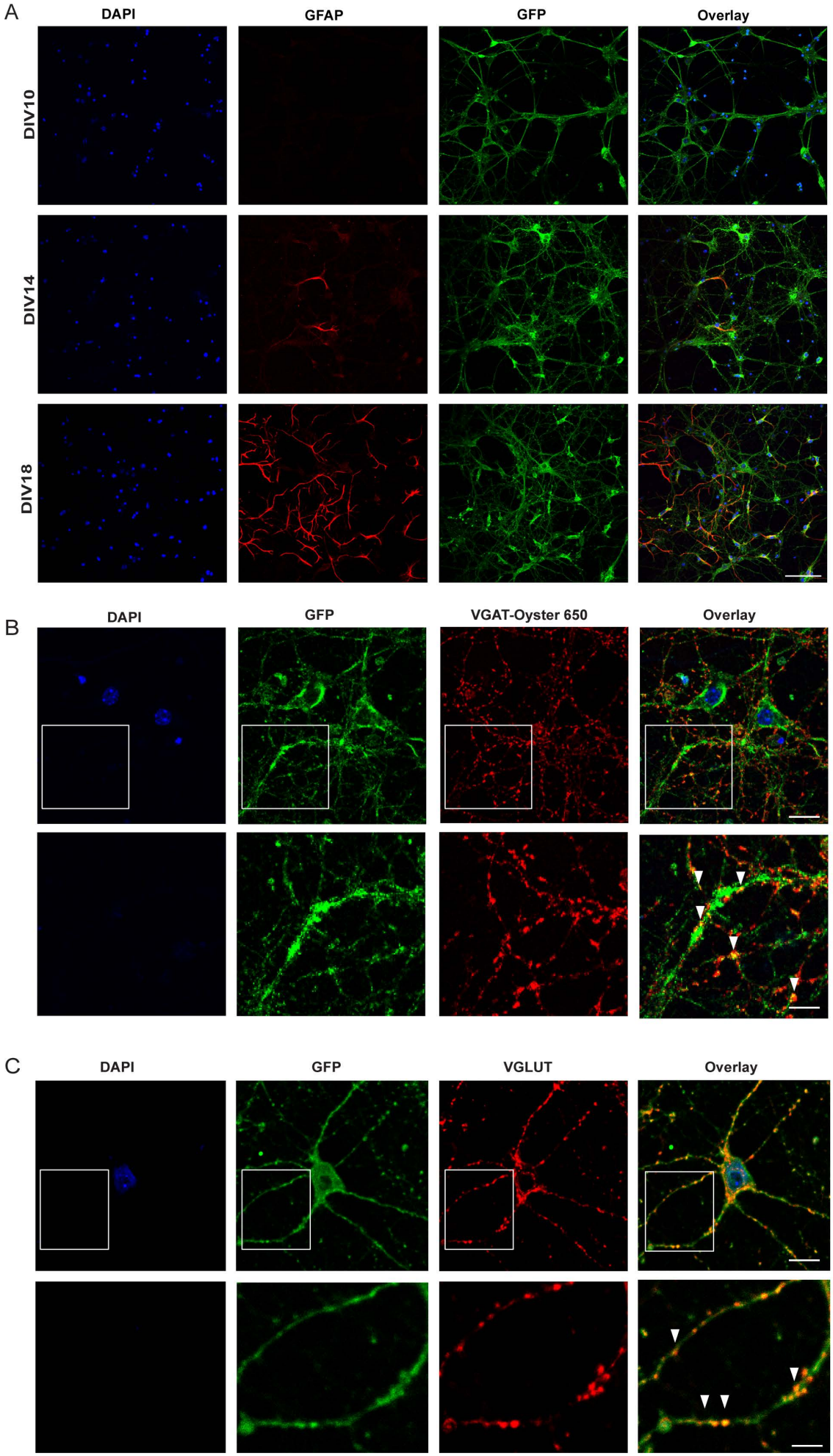

Figure S2. ex.E^{2}GFP expression pattern in vitro. A. ex.E^{2}GFP-infected neurons were fixed and stained with antibodies to GFP (green), glial fibrillary acidic protein (GFAP, red) and DAPI for nuclei. Between DIV 10-14, very few GFAP-positive cells were present. More glial cells were present at DIV 18; however also at this stage no significant expression of ex.E^{2}GFP in GFAP-positive cells was detected. Scale bars, 20 μm. **B.** Representative images of primary cortical neurons infected with ex.E^{2}GFP and stained for GFP (green), VGAT-oyster 650 (red) and DAPI (blue), to monitor expression of the probe in inhibitory neurons/terminals. Scale bars, 20 μm and 10 μm for low (upper row) and high (lower row) magnification, respectively. **C.** Representative images of primary cortical neurons infected with ex.E^{2}GFP and stained for GFP (green), VGLUT (red) and DAPI (blue), to monitor expression of the probe in excitatory neurons/terminals. Scale bars, 20 μm and 5 μm for low (upper row) and high (lower row) magnification, respectively.

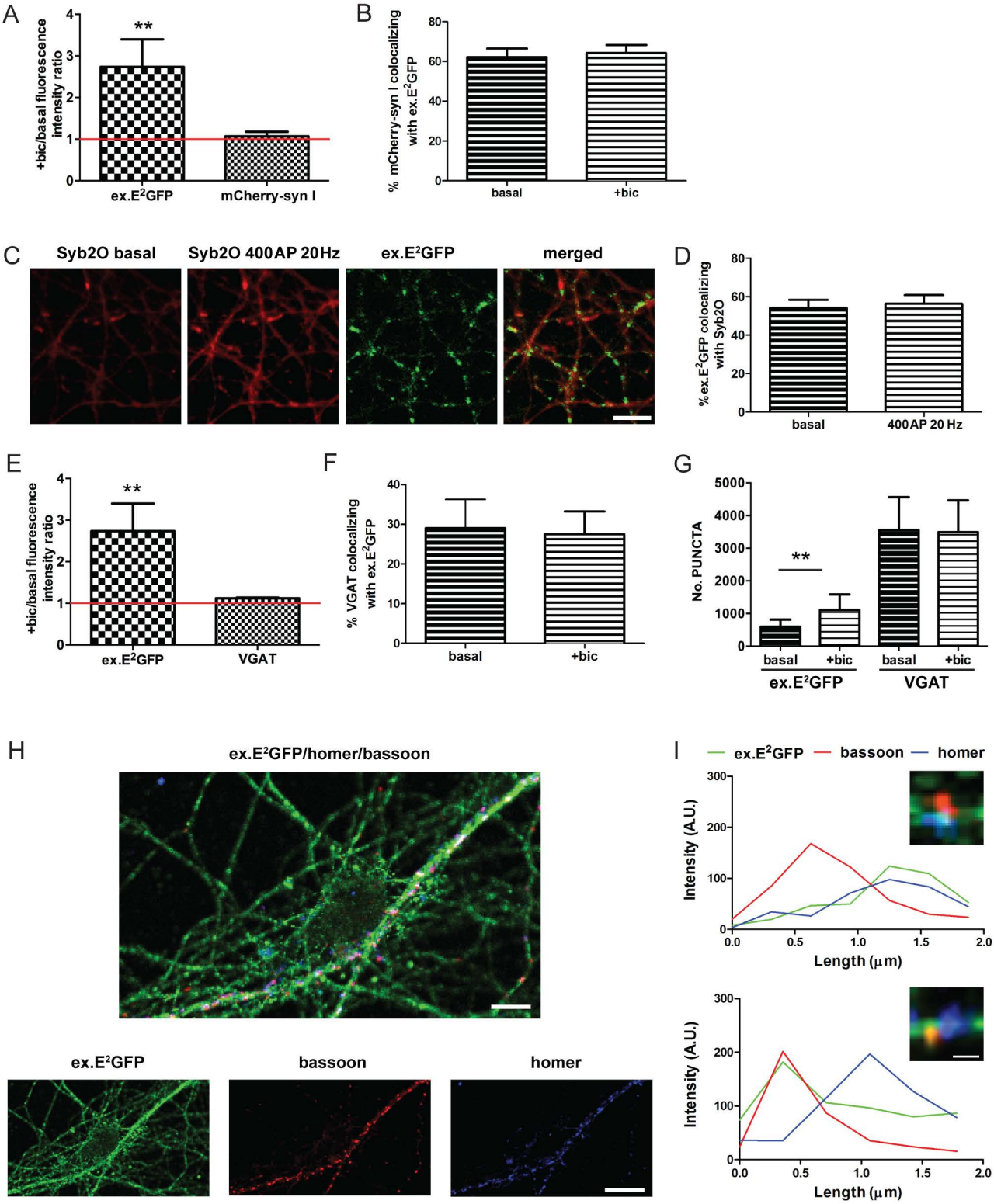

Figure S3. ex.E^{2}GFP-positive puncta increase in number and intensity after bicuculline stimulation.

A. Primary cortical neurons were co-infected at DIV7 with ex.E^{2}GFP and mCherry-syn I expressing viruses. Quantitative evaluation of ex.E^{2}GFP and mCherry syn I fluorescence intensity after bicuculline treatment (+*bic*) was measured and normalized to the values of untreated samples, set to 1 (red line); n = 5 fields from 3 independent experiments. **B.** Quantification of the fraction of the mCherry-syn I area that overlapped with ex.E^{2}GFP positive fluorescence under basal and bicuculline conditions evaluated as Mander's coefficient is given as means ± sem (n = 5 fields from 3 independent experiments). No significant differences were observed. **C,D. C.** Primary cortical neurons were co-infected at DIV13 with ex.E^{2}GFP and synaptobrevin-pHluorin m-Orange2 (Syb2O) expressing viruses. Optical recordings were performed at DIV 17-18. Representative images of ex.E^{2}GFP and Syb2O fluorescence under basal conditions and after electrical stimulation (1200 AP, 20 Hz). Scale bar, 5 µm. **D.** Quantification of ex.E^{2}GFP/Syb2O colocalization evaluated as Manders's coefficient (n = 11 fields from 3 independent experiments). No significant differences were observed. **E.** ex.E^{2}GFP infected neurons were stained with VGAT-oyster650 and quantitative evaluation of ex.E^{2}GFP and VGAT-oyster650 fluorescence intensity after bicuculline treatment (+*bic*) was measured and normalized to the values of untreated samples, set to 1 (red line); n = 4 fields from 3 independent experiments. **F.** Quantification of the fraction of Oyster-VGAT650 puncta that overlapped with ex.E^{2}GFP fluorescence evaluated as Mander's coefficient under basal and bicuculline conditions, respectively (means ± sem of n = 6 fields from 3 independent experiments). No significant differences were observed. **G.** Density of ex.E^{2}GFP and VGAT-oyster650 positive puncta under basal (*basal*) conditions and after bicuculline treatment (+*bic*); n = 5 fields from 3 independent experiments. Data are means ± sem, **p < 0.01, one-way ANOVA and Bonferroni's post-hoc test. **H,I. H.** Representative images of primary neurons infected with ex.E^{2}GFP and stained for GFP (green), bassoon (red) and homer (blue), to monitor expression of the probe at pre- or post- synaptic membranes. Scale bar, 10 µm. **I.** Intensity profiles of ex.E^{2}GFP at single synaptic puncta in which pre- and post-synaptic signals did not completely overlap. Representative images of synaptic puncta analyzed are shown (top right). Scale bar, 1 µm.

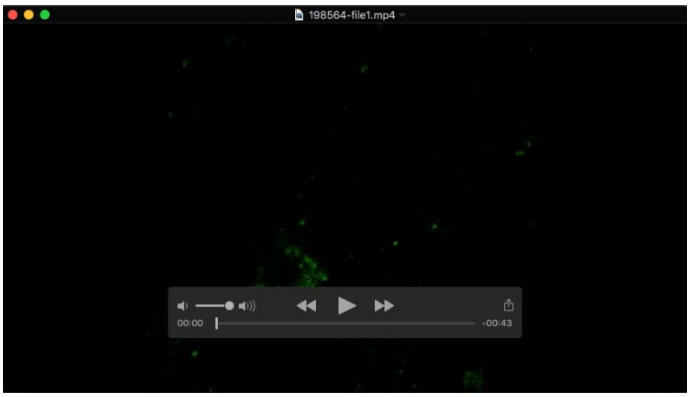

Movie S1: pH fluctuations upon network hyperactivity

Neurons were imaged by time-lapse fluorescence microscopy at λ_{ex} = 405 nm (1 image/2.58 s, total time: 1320 s, movie played at 29 frames/s) under basal conditions and after administration of bicuculline (30 μM) and TTX (300 nM).

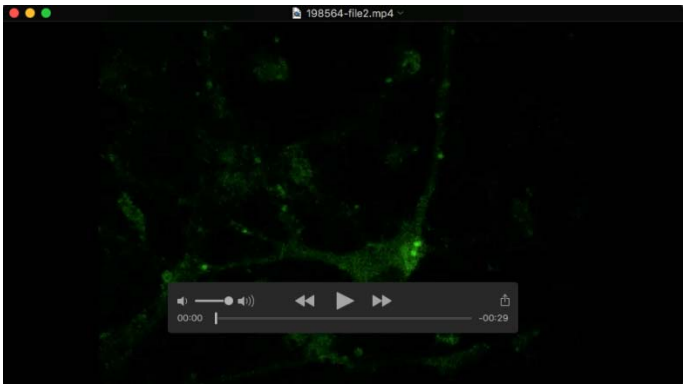

Movie S2: pH fluctuations upon high frequency stimulation

Neurons were imaged by time-lapse fluorescence microscopy, at λ_{ex} = 405 nm (1 image/2.58 s, total time: 350 s, movie played at 29 frames/s) under high frequency electrical stimulation (1200 AP, 10 Hz).